J. Nonlinear Sci. Vol. 11: pp. 239–277 (2001)
DOI: 10.1007/s00332-001-0392-x

Nonlinear Science

© 2001 Springer-Verlag New York Inc.

Pattern-Forming Systems for Control of Large Arrays of Actuators

E. W. Justh and P. S. Krishnaprasad
Institute for Systems Research and Department of Electrical and Computer Engineering, University of Maryland, College Park, MD 20742, USA
e-mail: justh@isr.umd.edu, krishna@isr.umd.edu

Received August 1, 2000; accepted August 16, 2001
Online publication November 5, 2001
Communicated by S. Wiggins

Summary. We consider an approach for coordinating the activity of a large array of microactuators via diffusive (i.e., nearest-neighbor) coupling combined with reactive growth and decay, implemented via *interconnection templates* which have been artificially engineered into the system (for example, in collocated microelectronic circuitry, or through the formulation of active material layers). Such coupled systems can support interesting spatiotemporal patterns, which in turn determine the actuation patterns. Generating such spatiotemporal patterns typically involves *stressing* the interconnections by raising or lowering a parameter resulting in the crossing of stability thresholds. The possibility of making such parametric adjustments via feedback on a slower timescale offers a solution to the problem of communicating effectively within a large array: The communication is achieved through the interconnection template. The mathematics behind this idea leads us into the rich domain of nonlinear partial differential equations (PDEs) with spatiotemporal pattern solutions. We present a global nonlinear stability analysis that applies to certain model pattern-forming systems. The nonlinear stability analysis could serve as a starting point for control system design for systems containing large microactuator arrays.

Key words. Nonlinear stability analysis, Lyapunov function, pattern-forming systems, activator-inhibitor equation, actuator arrays

1. Introduction

Recent technological advances in fabrication at the micro- and meso-scale suggest new ways to control *physical fields* (including flow, electrical, magnetic, and optical fields), thereby leading to new control problems involving the coordination of large arrays of

say, 10^4 to 10^6 microactuators, possibly also incorporating information from large arrays of collocated sensors. The microactuator arrays could be based on microelectromechanical systems (MEMS) technology; or materials which are electrically, magnetically, or optically active; or devices incorporating such materials, as in liquid-crystal light valves. The sensor arrays could also be based on MEMS or active materials, and if (coherent) light is used (either as the physical field to be controlled or as a measurement probe), a camera could serve as a sensor array. A common feature in these types of control problems is that, while there are very large numbers of actuators (and sensors), each one of these actuators/sensors is relatively simple. Further, control algorithms based on centralized processing of data become impractical on the scales under discussion.

To simplify the mathematical description of such actuator/sensor systems, it is natural to pass to the continuum limit (i.e., to consider partial differential equation models instead of high-order ordinary differential equation models) and to consider parallel, distributed control schemes. It is also essential that control system design and actuator array design be performed together, particularly when nonlinearity will play an essential role. There are two reasons that nonlinearity can appear in these control problems: either nonlinearity is present for fundamental physical reasons related to the application (such as in coherent optics when optical phase is being controlled, but intensity is being measured), or else the nonlinearity is incorporated explicitly to achieve richer behaviors in the system than can be obtained from a linear system. In many cases, both sources of nonlinearity would be present.

We are thus led to consider control of nonlinear PDE systems. Even before considering control, however, we are faced with the challenge of analyzing (and concurrently designing) such systems. In some cases, the control problem is clearly posed: for example, for adaptive optic phase distortion suppression, the actuator array is a spatial light modulator (SLM), and the control objective is to drive the SLM so as to compensate for (i.e., cancel) the phase distortion present in the coherent optical input beam. However, one can envision other types of microactuator array applications for which the selection of desired system trajectories is part of the design process, and these systems are the ones for which this work is potentially most relevant. Such actuator arrays could serve to manipulate meso-scale particles, pump/meter/mix fluids, interact with coherent structures in fluids, modulate acoustic radiation or optical fields, etc. [1]–[8].

The approach we consider for coordinating the activity of a large microactuator array involves diffusive (i.e., nearest-neighbor) coupling combined with reactive growth and decay, implemented via interconnection templates which have been artificially engineered into the system (for example, in collocated microelectronic circuitry, or through the formulation of active material layers). Such systems can support interesting spatiotemporal patterns, which in turn determine the actuation patterns. Generating such spatiotemporal patterns typically involves stressing the interconnections by raising or lowering a parameter resulting in the crossing of stability thresholds. The possibility of making such parametric adjustments via feedback on a slower timescale offers a solution to the problem of communicating effectively with a large array: The communication is achieved through the interconnection template.

The mathematics behind the above idea leads us into the rich domain of nonlinear partial differential equations with spatiotemporal pattern solutions. Pattern-forming systems are used to model diverse phenomena from biology, chemistry, and physics, and there

is an extensive body of both theoretical and experimental work on these systems. Biological examples include models for describing population dynamics, animal coloration patterns, various aspects of nervous systems, human visual hallucination patterns, and cardiac fibrillation [8], [9], [10], [11]. Examples from chemistry include certain catalyzed reactions, as in the catalytic converters used to convert carbon monoxide to carbon dioxide [8], [12]–[14]. Examples from physics include patterns observed in shaken collections of small spherical particles, gas discharge tubes, semiconductor electron-hole plasmas, Josephson-junction arrays, fluid convection, and optics [7], [8], [15]–[22]. Despite the diversity of underlying phenomena, all such pattern-forming systems share certain basic mathematical features, as reflected in the similarities among the observed patterns. All of the above are in the category of *analytical* approaches. In contrast, in recent work of Zhu and Mumford [23], a *synthetic* approach is taken (to discover reaction-diffusion equations) to solve the problems of computer vision, image processing, and graphics, suggesting role for nonlinear PDEs of the reaction-diffusion type in pattern synthesis, denoising, image enhancement, and clutter removal.

The philosophy underlying the study of pattern formation is that while each of the various physical systems has its own unique characteristics, certain basic features of the pattern-forming behavior are universal; i.e., independent of the details of the model. However, given some physical model that is known to exhibit patterns, it is not generally clear how to extract the part responsible for the pattern-forming behavior. Therefore, the standard approach to studying patterns is to write down simplified model equations, which do not necessarily have a specific physical origin, but which can be shown analytically to give rise to the patterns under study.

For the interconnection templates used to control actuator arrays, in the continuum limit, we first consider a certain *activator-inhibitor* system which also happens to serve as a model equation for a variety of pattern phenomena. This system has the property that as a bifurcation (or control) parameter passes through a critical value, a stable spatially uniform solution gives way to a stable pattern solution (having spatial variation, time variation, or both). Besides the spatially uniform solution and various pattern solutions, other interesting solutions can also be excited in these systems, such as spatially localized (finite-amplitude) spike states [24], [25].

This paper contributes an approach to global nonlinear stability analysis for certain model pattern-forming systems including the activator-inhibitor equations mentioned above. This nonlinear stability analysis could serve as a starting point for control system design. The message, perhaps somewhat surprising, is that a global nonlinear stability analysis is possible for certain nonlinear PDE systems with interesting pattern solutions.

Although the pattern-forming-system approach for controlling actuator arrays involves PDEs, it differs fundamentally from the usual approaches for control of PDEs, e.g., as expressed by Lions [26]. In conventional PDE control problems, the PDE has a physical origin (e.g, the Navier-Stokes equation), and it is only physically meaningful to consider boundary control, or control at limited parts of the interior of the domain. By contrast, the PDE modeling an actuator array and its control circuitry describes an engineered system, and control throughout the domain (e.g., from collocated sensors) is not only possible, but is very much of interest. Adaptive optics presents a prime example of this [27], [28].

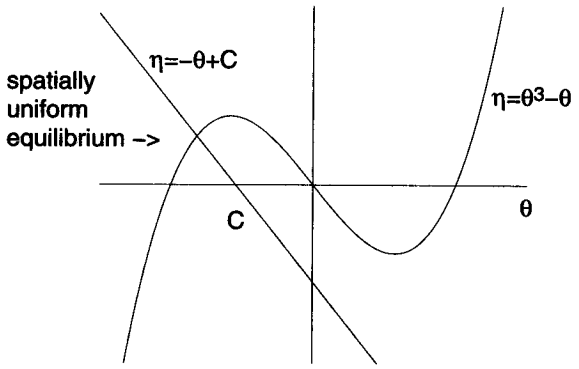

Fig. 1. The intersection of the curves $\eta(\theta) = \theta^3 - \theta$ and $\eta(\theta) = -\theta + C$ determines the spatially uniform equilibrium of equation 1.

We begin (in Section 2) by introducing the activator-inhibitor model and discussing its qualitative behavior. We also discuss a discrete analog network realization of this model. Then we present the mathematical analysis in Sections 3 and 4, leading to a class of Lyapunov functions inspired by classical lumped electrical network analysis, as in the work of Robert Brayton and Jürgen Moser [31]. In Section 5 we discuss some other systems which are related mathematically to the basic model and sketch how our analysis extends to these systems. Finally, in Section 6, we use coherent optics as an example for illustrating the concurrent design and analysis approach for achieving global nonlinear stability in systems with large arrays of actuators and sensors.

2. Activator-Inhibitor Equations and Their Solutions

The systems we consider here are related to the cubic nonlinearity activator-inhibitor system,

$$\begin{aligned} \tau_\theta \frac{\partial \theta}{\partial t} &= l^2 \Delta\theta - \theta^3 + \theta + \eta, \\ \tau_\eta \frac{\partial \eta}{\partial t} &= L^2 \Delta\eta - \eta - \theta + C, \end{aligned} \tag{1}$$

where $\theta(\mathbf{x}, t)$ is the activator, $\eta(\mathbf{x}, t)$ is the inhibitor, l, L, τ_θ, and τ_η are positive constants, C is the control (or bifurcation) parameter, and Δ represents the Laplacian operator. The ratio of time constants, $\alpha = \tau_\theta/\tau_\eta$, and the ratio of lengthscales, $\beta = l/L$, are the parameters primarily responsible for the pattern-forming properties of system (1). Although the mathematical results we discuss hold for $\mathbf{x} \in \mathbb{R}^n$ for any n, for the potential applications we have in mind, $n = 2$, and $\Delta = \partial^2/\partial x^2 + \partial^2/\partial y^2$. The system has a spatially uniform equilibrium solution given by the intersection of the curve $\eta(\theta) = \theta^3 - \theta$ with the line $\eta(\theta) = -\theta + C$, as shown in Figure 1.

We are primarily interested in $\beta \ll 1$, in which case the spatially uniform equilibrium solution is stable for $|C| > \frac{1}{3\sqrt{3}}$. When the spatially uniform equilibrium solution is

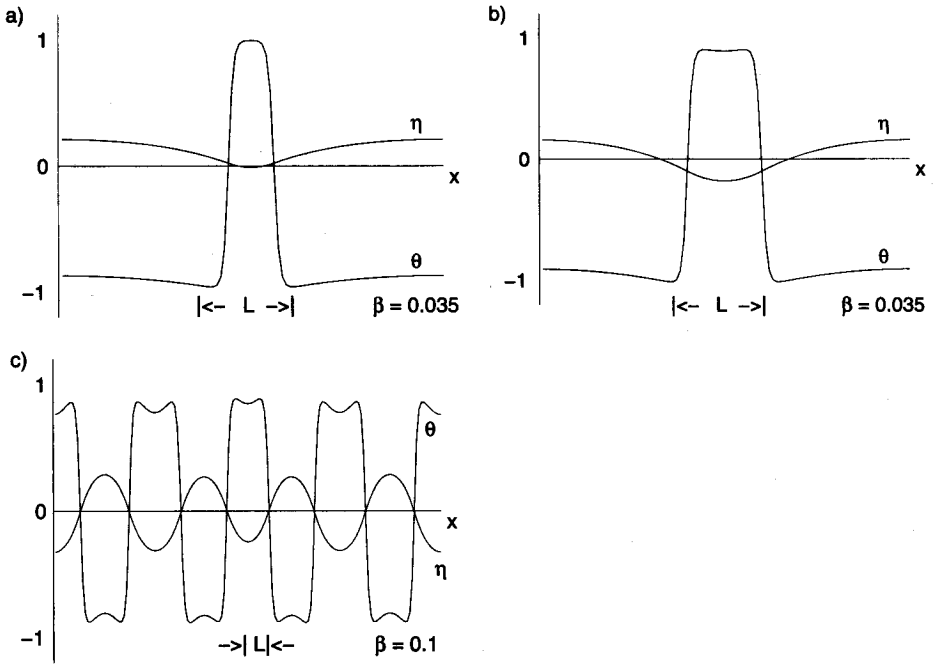

Fig. 2. Stable equilibria of equation (1) for $n = 1$: (a) narrow spike equilibrium, (b) wide spike equilibrium, (c) pattern equilibrium. In (a) and (b), $C = -\frac{2\sqrt{2}}{3\sqrt{3}}$, and in (c), $C = 0$. The boundary conditions are periodic.

unstable, a pattern solution is stable. When $\alpha \ll 1$, there is an ideal pattern solution which is periodic in both space and time. However, for the case we are primarily interested in, $\alpha > 1$, the ideal pattern solutions are spatially periodic equilibria. Furthermore, when $\beta \ll 1$ and $\alpha > 1$, other equilibria may also be stable. Various equilibria for $n = 1$ are shown in Figure 2; those for $n = 2$ are shown in Figure 3.

Actual patterns observed in pattern-forming systems generally differ from the ideal patterns, unless at least one of several special conditions is met:

- the system is highly homogeneous and is uniformly maintained very close to the bifurcation point where stability of the spatially uniform equilibrium has just given way to stability of the pattern solution;
- the system is excited into the pattern state in a carefully controlled way so that the ideal pattern is obtained; or
- there is long-range coupling present so that an ideal pattern is energetically favorable as compared with a more disordered pattern.

Unless one of these special conditions is met, the actual pattern observed looks locally like the ideal pattern, but exhibits disorder over long ranges, as illustrated in Figure 3b.

The factors that influence actual patterns are initial conditions, boundary conditions, inhomogeneities, and symmetry breaking. Initial conditions, boundary conditions, and inhomogeneities might be used for pattern control. (During symmetry breaking, tiny

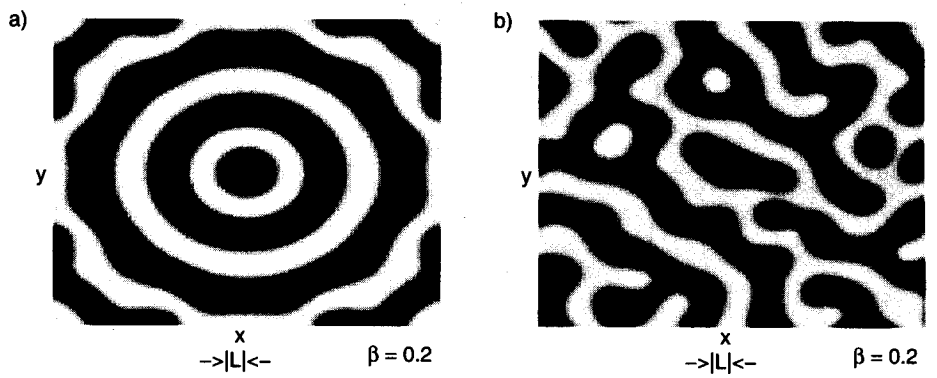

Fig. 3. Stable equilibria of equation (1) for $n = 2$ and $C = 0$: (a) a radially symmetric pattern, and (b) an irregular pattern. In (a), the radial symmetry of the pattern breaks down toward the edges of the domain due to the periodic boundary conditions. Spike solutions and wall solutions, analogous to Figures 2a and 2b, and an ideal pattern consisting of parallel rolls, analogous to Figure 2c, are also possible (but not shown).

perturbations beyond our control select the position and orientation of the pattern.) Although ideal patterns have been the focus of much of the theoretical and experimental work with pattern-forming systems, the fact that actual patterns have the flexibility to deviate from ideal patterns means that a rich variety of patterns can be realized.

For the cubic nonlinearity model with $\beta \ll 1$ and $\alpha > 1$, both the pattern regime and the spike regime might be useful, depending on the particular application. Two surfaces with micro-actuator arrays in contact with each other could change the coefficient of friction between them by alternating between the spatially uniform equilibrium state (low friction), and a state of disordered interlocking rolls (high friction), under the control of a parameter common to all of the actuators. Alternatively, interlocking patterns of parallel rolls would produce a high coefficient of friction normal to the rolls, and low friction in the direction parallel to the rolls. In the friction example, the pattern regime would be the regime of interest. An analog memory (discussed below), in which spikes are excited by collocated sensor signals, is an application where the spike regime would be of interest.

2.1. Exciting Spikes Using the Control Parameter

One technique for exciting a spike is to locally raise the control parameter above the bifurcation threshold. When the control parameter is in the pattern-forming regime over a localized region, the pattern solution forms in that region but smoothly connects to the spatially uniform equilibrium outside that region. When the control parameter is then returned to the below-threshold value, the pattern solution relaxes to the corresponding spike solution. This method of exciting spikes is illustrated for one dimension in Figure 4 and for two dimensions in Figure 5. If the control parameter is raised over a larger region than required to excite a single spike, then there are various possibilities, depending on the shape of the region in which the control parameter was raised and on the spatially uniform value of control parameter to which the system is returned [17]. Some possibilities are

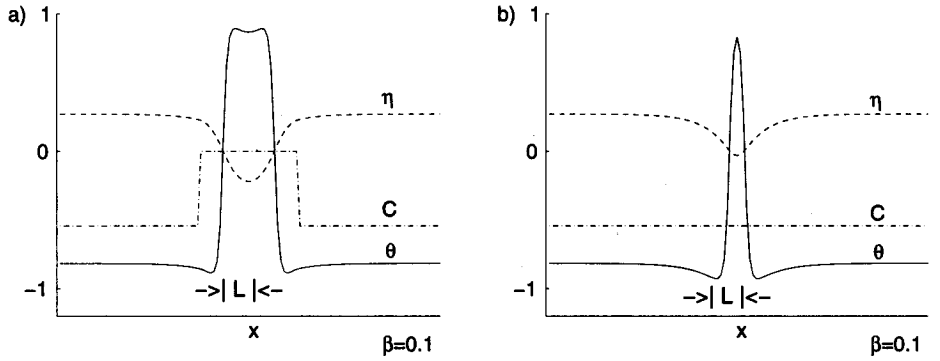

Fig. 4. (a) One cycle of the pattern solution excited by locally raising the control parameter for the one-dimensional system, and (b) the resulting spike equilibrium when the control parameter is restored to its spatially uniform value. $C = -\frac{2\sqrt{2}}{3\sqrt{3}}$ is the spatially uniform value and $C = 0$ is the locally elevated value of the control parameter.

shown in Figure 6. Once spike solutions have been excited in various locations, they can all be removed at once simply by taking the control parameter to a value where only a spatially uniform equilibrium is stable.

Since the control parameter needs to be raised only temporarily in a localized region to excite a spike, a sensor-driven mechanism for exciting a spike can be ac-coupled. A network can thereby act as an analog memory, forming spikes asynchronously and in parallel in response to local sensor driving. Given a spatial distribution of spikes (or circular walls, as in Figure 6), any interaction between them decreases exponentially with distance [21]. Therefore, unless the activator-inhibitor system is highly homogeneous, one would not expect to observe interactions between spikes or walls that are not in close proximity. However, numerical study indicates that under some conditions in highly homogeneous systems, spikes can attract or repel each other, creating complicated "molecules," and similar results have been observed in gas discharge experiments [21]. Even in systems that are homogeneous enough for spikes to influence each other, for

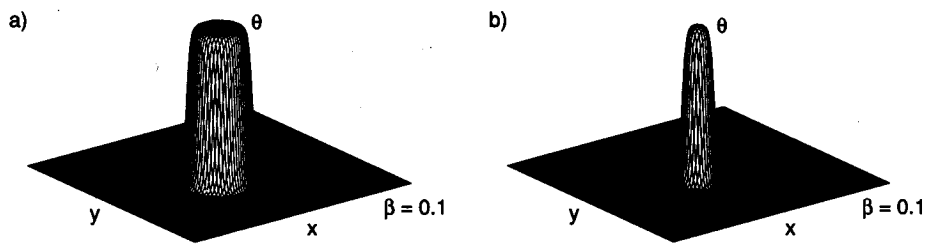

Fig. 5. (a) One cycle of the pattern solution excited by locally raising the control parameter for the two-dimensional system, and (b) the resulting spike equilibrium when the control parameter is restored to its spatially uniform value. $C = -\frac{2\sqrt{2}}{3\sqrt{3}}$ is the spatially uniform value and $C = 0$ is the locally elevated value of the control parameter.

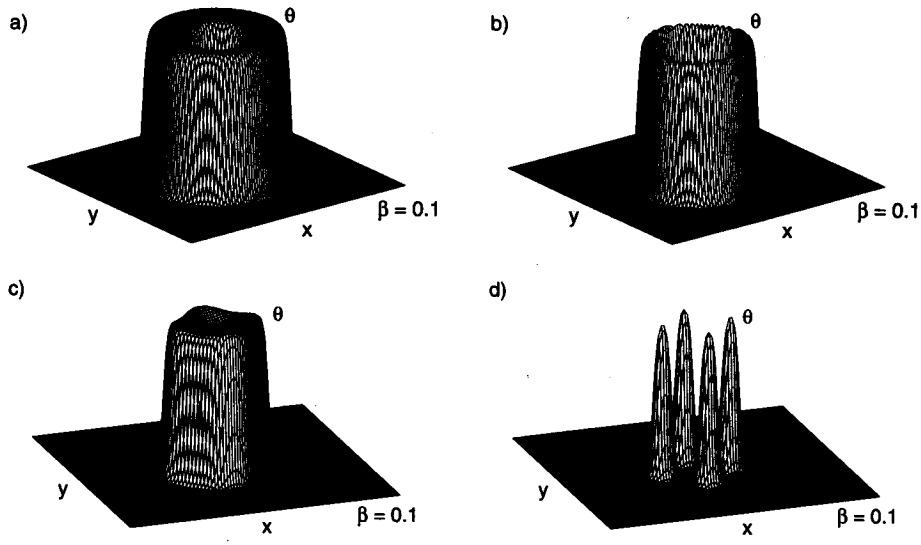

Fig. 6. (a) Response to a local increase in the control parameter over a circular region larger than in Figure 5a, and (b) the resulting circular wall equilibrium when the control parameter is restored to its spatially uniform value. (c) Response to a local increase in the control parameter over a region which is not circularly symmetric, and (d) the resulting spikes when the control parameter is restored to its spatially uniform value. As in Figure 5, $C = -\frac{2\sqrt{2}}{3\sqrt{3}}$ is the spatially uniform value and $C = 0$ is the locally elevated value of the control parameter.

spikes separated by a sufficiently large distance, the resulting motion of the spikes is on a much longer timescale than τ_θ and τ_η (when $\tau_\theta > \tau_\eta$, but $\tau_\theta \approx \tau_\eta$).

2.2. *Advecting Spikes*

For $\beta \ll 1$ and $\alpha > 1$, the stable solutions for the cubic nonlinearity model are equilibria. When $\alpha \ll 1$, time-periodic patterns and traveling spikes are also possible. However, the pattern-selection problem (i.e., the problem of selecting stationary versus traveling spikes and prescribing the direction the traveling spikes travel) is quite difficult. There are, however, alternative approaches to taking $\alpha \ll 1$ in the cubic nonlinearity model in order to obtain interesting time-varying patterns of activity in an array of actuators. One approach is simply to add an additional advective term to the dynamics:

$$\begin{aligned} \tau_\theta \frac{\partial \theta}{\partial t} &= l^2 \Delta\theta - \theta^3 + \theta + \eta, \\ \tau_\eta \frac{\partial \eta}{\partial t} &= L^2 \Delta\eta - \eta - \theta + C + L(\boldsymbol{\varepsilon} \cdot \nabla\eta), \end{aligned} \tag{2}$$

where $\boldsymbol{\varepsilon}$ is a constant vector, ∇ denotes the gradient with respect to $\mathbf{x}$, and here the dot denotes the inner product of vectors. If $||\boldsymbol{\varepsilon}||$ is sufficiently small, the spike shape in Figure 5b is slightly distorted, and the spike translates, as shown in Figure 7.

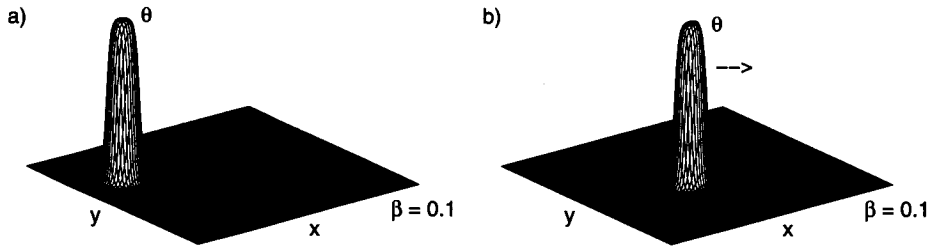

Fig. 7. (a) Initial excitation, and (b) resulting traveling spike for system (2). The traveling spike is a slightly distorted, translating version of the spike shown in Figure 5b.

2.3. Electronic Circuit Implementation

A digital implementation of the spatially discretized activator-inhibitor dynamics might be possible when relatively large MEMS actuators are to be controlled. The actuators would have to be large because of the area required for digital circuitry to perform the calculations at each site. At the expense of greater complexity, one could also design a digital implementation in which a number of actuators shared the same computational circuitry in order to keep the area of the digital circuitry small enough. Besides the usual advantages of a digital approach, such as simple biasing and highly accurate computations, the uniformity across the array would make it possible to work with the pattern-forming system very close to the bifurcation threshold.

However, an analog implementation would inherently lack the uniformity required to operate very close to the bifurcation threshold, since analog circuits are sensitive to processing variations that lead to device nonuniformities. The main advantage of an analog implementation, however, is compact size, and if the actuators are small enough, an analog approach might be preferred for that reason. There are different forms that an analog implementation could take, but a simple approach is to consider both θ and η to be voltages, as shown in Figure 8.

From Figure 8, the equations for θ_k and η_k are

$$\begin{aligned}(\tau_\theta\delta)\frac{d\theta_k}{dt} &= \frac{l^2}{\delta}(\theta_{k+1}-\theta_k)+\frac{l^2}{\delta}(\theta_{k-1}-\theta_k)-(\theta_k^3-2\theta_k+C)\delta+(\eta_k-\theta_k)\delta,\\ (\tau_\eta\delta)\frac{d\eta_k}{dt} &= \frac{L^2}{\delta}(\eta_{k+1}-\eta_k)+\frac{L^2}{\delta}(\eta_{k-1}-\eta_k)+(-\theta_k-\eta_k)\delta,\end{aligned} \tag{3}$$

which simplify to

$$\begin{aligned}\tau_\theta\frac{d\theta_k}{dt} &= \frac{l^2}{\delta^2}(\theta_{k+1}-2\theta_k+\theta_{k-1})-\theta_k^3+\theta_k+\eta_k-C,\\ \tau_\eta\frac{d\eta_k}{dt} &= \frac{L^2}{\delta^2}(\eta_{k+1}-2\eta_k+\eta_{k-1})-\eta_k-\theta_k.\end{aligned} \tag{4}$$

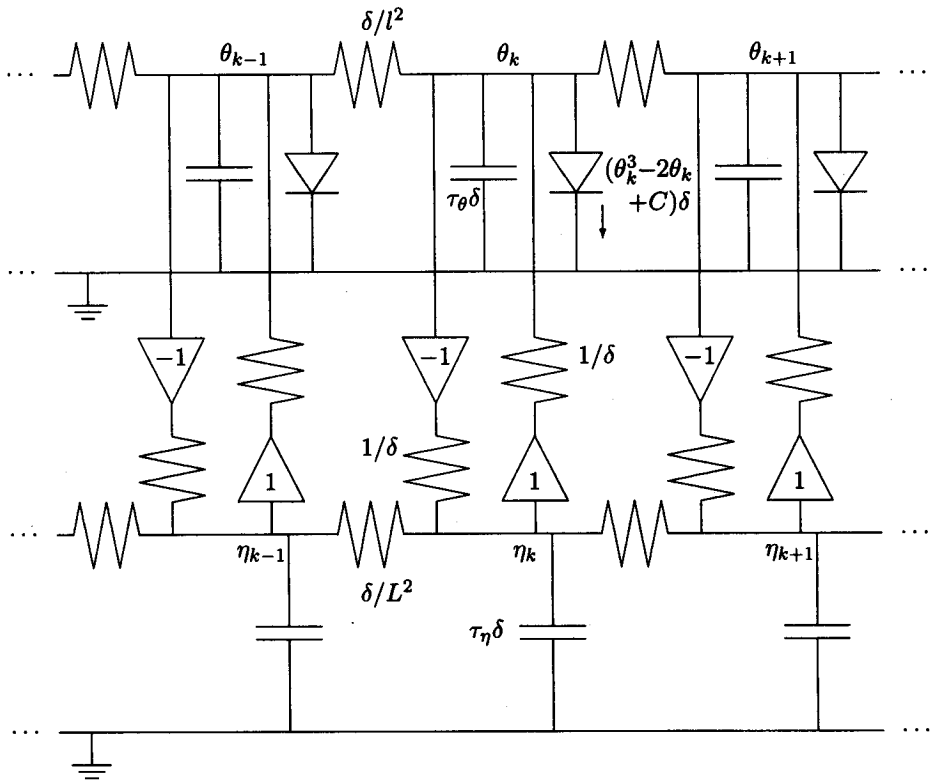

Fig. 8. An implementation of the spatially discretized cubic nonlinearity model dynamics in which the θ_k and η_k are voltages. Resistive coupling implements the diffusion, capacitors produce the time constants, inverting and noninverting buffers provide the cross-coupling, and active elements (shown as diode symbols, representing tunnel diodes) provide the nonlinearity and positive feedback. The tunnel-diode biasing circuitry is not shown.

In the continuum limit (i.e., taking $\delta \to 0$), these equations become

$$\begin{aligned} \tau_\theta \frac{\partial \theta}{\partial t} &= l^2 \frac{\partial^2 \theta}{\partial x^2} - \theta^3 + \theta + \eta - C, \\ \tau_\eta \frac{\partial \eta}{\partial t} &= L^2 \frac{\partial^2 \eta}{\partial x^2} - \eta - \theta. \end{aligned} \tag{5}$$

The control parameter can be moved to the inhibitor equation by taking $\tilde{\eta} = \eta - C$ (although there is no problem with having the control parameter in the activator equation as opposed to the inhibitor equation). The circuit of Figure 8 generalizes to two dimensions by making the resistor and capacitor grids two-dimensional.

An analog network essentially implementing the cubic nonlinearity model was built by Purwins and Radehaus [22]. In their circuit, the inhibitor was the voltage across a capacitor and the activator was the current through an inductor; therefore, the nonlinearity had to be implemented as an S-shaped current-voltage characteristic. (The analog

network of Purwins and Radehaus was designed the way it was because of the physical analogy with gas discharge systems, and because the implementation used discrete components rather than integrated circuit technology. In our setting, we are not so constrained.)

3. Basic Properties of Solutions

3.1. Existence, Uniqueness, and Regularity

The purpose of this section is to present mathematically rigorous statements concerning the cubic nonlinearity model. The cubic nonlinearity model belongs to a general class of models

$$\begin{aligned} \tau_\theta \frac{\partial \theta}{\partial t} + L_\theta \theta + f_\theta(\theta) &= \eta, \\ \tau_\eta \frac{\partial \eta}{\partial t} + L_\eta \eta + f_\eta(\eta) &= -\theta, \end{aligned} \tag{6}$$

defined on an open bounded subset $\Omega \subset \mathbb{R}^n$, where L_θ and L_η are uniformly parabolic operators, and $f_\theta(\theta)$ and $f_\eta(\eta)$ are odd-order polynomials with positive leading coefficients. Suppose also that the boundary conditions are one of the three basic types:

1. Dirichlet: $\theta(\mathbf{x}, t) = 0, \quad \eta(\mathbf{x}, t) = 0$ on $\partial\Omega$,
2. Neumann: $\nabla\theta \cdot \mathbf{n} = 0, \quad \nabla\eta \cdot \mathbf{n} = 0$ on $\partial\Omega$ where $\mathbf{n}$ is normal to $\partial\Omega$, or
3. periodic boundary conditions.

Also, suppose the initial data $(\theta(0), \eta(0)) \in L^2(\Omega) \times L^2(\Omega)$. Using the standard techniques for proving existence and uniqueness for parabolic PDEs, one can prove that the above system of PDEs has a unique weak solution $(\theta(\mathbf{x}, t), \eta(\mathbf{x}, t))$, with

$$\begin{aligned} \theta &\in L^\infty(0, T; L^2(\Omega)) \cap L^2(0, T; H(\Omega)) \cap L^{2p_\theta}(0, T; L^{2p_\theta}(\Omega)), \\ \eta &\in L^\infty(0, T; L^2(\Omega)) \cap L^2(0, T; H(\Omega)) \cap L^{2p_\eta}(0, T; L^{2p_\eta}(\Omega)), \end{aligned} \tag{7}$$

where $2p_\theta - 1$ is the degree of $f_\theta(\theta)$, $2p_\eta - 1$ is the degree of $f_\eta(\eta)$, and $H(\Omega)$ is the appropriate Sobolev space corresponding to the boundary conditions (e.g., $H(\Omega) = H_0^1(\Omega)$ for Dirichlet boundary conditions) [29], [30]. In addition to existence and uniqueness of solutions, the solutions also depend continuously on the initial data.

If we have the further assumptions that the boundary $\partial\Omega$ is C^2 and that $(\theta(0), \eta(0)) \in L^{2p_\theta}(\Omega) \times L^{2p_\eta}(\Omega)$, then we can show further that

$$\begin{aligned} D^2\theta &\in L^2(0, T; L^2(\Omega)), \\ D^2\eta &\in L^2(0, T; L^2(\Omega)), \end{aligned} \tag{8}$$

which implies

$$\begin{aligned} \theta &\in L^2(0, T; H^2(\Omega)), \\ \eta &\in L^2(0, T; H^2(\Omega)), \end{aligned} \tag{9}$$

with $H^2(\Omega)$ corresponding to $H(\Omega)$ defined in the appropriate way. These bounds on the second partial derivatives of θ and η are what we mean by "regularity." We will require this amount of regularity in the calculations that follow. The restriction that the coupling between the θ and η equations is linear is used in the proofs of existence, uniqueness, and regularity.

3.2. Dissipativity

For finite-dimensional systems, the physical notion of dissipativity can be tied to the mathematical concept of the existence of an absorbing set. For infinite-dimensional systems, it is not so clear how dissipativity should be precisely defined, since there are systems which are considered "dissipative," but for which the existence of absorbing sets has not been established [30]. However, if for an infinite-dimensional system we can prove the existence of an absorbing set, we can certainly label the system dissipative, and the cubic nonlinearity model does possess an absorbing set. The energy bounds required to show the existence of an absorbing set are stronger than those required to show existence, uniqueness, and regularity of solutions.

Let $\mathbf{u}(t) = (\theta(t), \eta(t))$ denote the solution for the cubic nonlinearity model, let $\mathbf{u}_0 = \mathbf{u}(0)$, and let $\mathbf{L} = L^2(\Omega) \times L^2(\Omega)$. Then the semigroup $\{S(t)\}_{t\geq 0}$ defined by

$$\begin{aligned} S(t)\colon \mathbf{L} &\to \mathbf{L}, \\ \mathbf{u}_0 &\to \mathbf{u}(t), \end{aligned} \tag{10}$$

is well-defined $\forall t \in [0, T]$ for T arbitrarily large. Note that $\mathbf{H} = (H(\Omega) \cap L^{2p_\theta}(\Omega)) \times (H(\Omega) \cap L^{2p_\eta}(\Omega)) \subset \mathbf{L}$ is the Hilbert space in which $\mathbf{u}(t)$ lies for almost every t. However, writing $S(t)\colon \mathbf{L} \to \mathbf{L}$ reflects the fact that our initial conditions only need to be in $\mathbf{L}$ for the existence and uniqueness theory to hold.

The semigroup $\{S(t)\}_{t\geq 0}$ satisfies the basic semigroup properties,

$$\begin{aligned} S(t+s) &= S(t) \cdot S(s) \quad \forall s, t \geq 0, \\ S(0) &= I \text{ (the identity)}, \\ \mathbf{u}(t+s) &= S(t)\mathbf{u}(s) = S(s)\mathbf{u}(t), \end{aligned} \tag{11}$$

and in addition, because of the continuous dependence of solutions on initial data, we have that $S(t)$ is a continuous operator $\forall t \geq 0$. A set $\mathcal{B} \subset \mathcal{U}$, where $\mathcal{U}$ is an open set in $\mathbf{L}$, is called an absorbing set in $\mathcal{U}$ if the orbit of any bounded set of $\mathcal{U}$ enters into $\mathcal{B}$ after a certain time (which may depend on the set); i.e., $\forall \mathcal{B}_0 \subset \mathcal{U}$, $\mathcal{B}_0$ bounded, $\exists t_1(\mathcal{B}_0)$ such that $S(t)\mathcal{B}_0 \subset \mathcal{B}$ $\forall t \geq t_1(\mathcal{B}_0)$. An attractor is a set $\mathcal{A} \subset \mathbf{L}$ such that

(i) $\mathcal{A}$ is invariant; i.e., $S(t)\mathcal{A} = \mathcal{A}$ $\forall t \geq 0$, and
(ii) $\exists \mathcal{U}$, open, such that $\forall \mathbf{u}_0 \in \mathcal{U}$, $S(t)\mathbf{u}_0 \to \mathcal{A}$ as $t \to \infty$; i.e., $\text{dist}(S(t)\mathbf{u}_0, \mathcal{A}) \to 0$ as $t \to \infty$.

The largest such $\mathcal{U}$ is the basin of attraction of $\mathcal{A}$. If the basin of attraction of $\mathcal{A}$ is all of $\mathbf{L}$, then $\mathcal{A}$ is a global attractor for $\{S(t)\}_{t\geq 0}$.

The existence of a global attractor implies the existence of an absorbing set. For the cubic nonlinearity model, the existence of an absorbing set implies the existence of an

attractor, due to the following theorem (which is a special case of a theorem due to Temam [30]; see [24] for a proof):

Theorem. *Suppose* $\mathbf{L}$ *is a Banach space and that the operators* $S(t)$ *satisfy the semigroup properties and are continuous operators from* $\mathbf{L}$ *into itself* $\forall t > 0$. *Suppose that there exists an open set* $\mathcal{U}$ *and a bounded set* $\mathcal{B}$ *of* $\mathcal{U} \cap \mathbf{H}$ *such that* $\mathcal{B} \subset \mathbf{H} \subset\subset \mathbf{L}$ *and* $\mathcal{B}$ *is absorbing in* $\mathcal{U}$. *Then the* ω*-limit set of* $\mathcal{B}$, $\mathcal{A} = \omega(\mathcal{B})$, *is a compact attractor which attracts the bounded sets of* $\mathcal{U}$. *It is the maximal bounded attractor. Furthermore, if* $\mathcal{U}$ *is convex and connected, then* $\mathcal{A}$ *is connected, too.*

Remark. By $\mathbf{H} \subset\subset \mathbf{L}$, for $\mathbf{H}$ and $\mathbf{L}$ Banach spaces, we mean $\mathbf{H}$ is compactly embedded in $\mathbf{L}$. For our $\mathbf{H}$ and $\mathbf{L}$, $\mathbf{H} \subset\subset \mathbf{L}$ follows from standard compactness theory [29].

So to demonstrate the dissipativity of the cubic nonlinearity model, we need to exhibit an absorbing set in $\mathbf{H}$. Such an absorbing set does exist for the cubic nonlinearity model. In fact, this absorbing set absorbs all the bounded sets of $\mathbf{H}$. The existence of this absorbing set then implies the existence of a global attractor by the above theorem. The details can be found in [24].

4. Derivation of a Lyapunov Functional

Since dissipation plays a crucial role in the behavior of activator-inhibitor equations, it is natural to try to apply energy methods. In fact, for the cubic nonlinearity model, it is easy to write down an energy functional $\tilde{V}$ for which the system is a gradient system, but with respect to an indefinite metric. It turns out that for the cubic nonlinearity model, this energy functional, for certain parameter values, leads us to find a radially unbounded Lyapunov functional V, with $\dot{V} \leq 0$, and with $\dot{V} = 0$ only at equilibrium points of the dynamics. This result is an infinite-dimensional generalization of a corresponding result of Brayton and Moser for systems of ODEs [25], [31].

To illustrate the technique of Brayton and Moser, we spatially discretize the cubic nonlinearity model to obtain a system of ODEs. The discretized dynamics are shown to be gradient dynamics with respect to an energy function, in analogy with the PDE system. The procedure of Brayton and Moser is then applied to the system of ODEs, yielding a Lyapunov function, provided the ratio of time constants, $\alpha = \tau_\theta/\tau_\eta$, is greater than one. Since the Lyapunov function V is radially unbounded and satisfies $\dot{V} \leq 0$ with $\dot{V} = 0$ only at equilibrium points of the dynamics, LaSalle's invariance principle enables us to conclude that all trajectories converge to the set of equilibrium points of the dynamics [33]. Furthermore, because V is analytic, it can be proved that each trajectory converges to an equilibrium [34], [35].

Having shown how the technique of Brayton and Moser applies to the discretized system of ODEs, we then show how the technique extends to the infinite-dimensional setting for the basic cubic nonlinearity model. Having obtained the Lyapunov functional for the cubic nonlinearity model, we then show how analogous Lyapunov functionals can be obtained for certain related systems.

4.1. *Gradient Dynamics Property of the Cubic Nonlinearity Model*

For the cubic nonlinearity model (1), there is an energy functional

$$\tilde{V} = \int_\Omega \left[\frac{l^2}{2}|\nabla\theta|^2 + \frac{1}{4}\theta^4 - \frac{1}{2}\theta^2 - \theta\eta - \frac{L^2}{2}|\nabla\eta|^2 - \frac{1}{2}\eta^2 + C\eta \right] d\mathbf{x}, \tag{12}$$

such that

$$\begin{aligned} \frac{d\tilde{V}}{dt} &= \frac{\delta\tilde{V}}{\delta\theta}\cdot\left(\frac{\partial\theta}{\partial t}\right) + \frac{\delta\tilde{V}}{\delta\eta}\cdot\left(\frac{\partial\eta}{\partial t}\right) \\ &= -\int_\Omega \left[\tau_\theta \left(\frac{\partial\theta}{\partial t}\right)^2 - \tau_\eta \left(\frac{\partial\eta}{\partial t}\right)^2 \right] d\mathbf{x} \\ &= -\left(\begin{bmatrix} \partial\theta/\partial t \\ \partial\eta/\partial t \end{bmatrix}, \begin{bmatrix} \tau_\theta & 0 \\ 0 & -\tau_\eta \end{bmatrix} \begin{bmatrix} \partial\theta/\partial t \\ \partial\eta/\partial t \end{bmatrix} \right). \end{aligned} \tag{13}$$

An equivalent way of expressing this is

$$-\tilde{J}\begin{bmatrix} \partial\theta/\partial t \\ \partial\eta/\partial t \end{bmatrix} = \nabla\tilde{V}, \quad \tilde{J} = \begin{bmatrix} \tau_\theta & 0 \\ 0 & -\tau_\eta \end{bmatrix}, \tag{14}$$

so that

$$\frac{d\tilde{V}}{dt} = \left(\nabla\tilde{V}, \begin{bmatrix} \partial\theta/\partial t \\ \partial\eta/\partial t \end{bmatrix} \right) = -\left(\begin{bmatrix} \partial\theta/\partial t \\ \partial\eta/\partial t \end{bmatrix}, \tilde{J}\begin{bmatrix} \partial\theta/\partial t \\ \partial\eta/\partial t \end{bmatrix} \right). \tag{15}$$

We thus have a gradient system with respect to an indefinite metric.

4.2. *Lyapunov Function Derivation for the Spatially Discretized Cubic Nonlinearity Model*

To see how the technique of Brayton and Moser works for ODE systems, consider the simplest discretization of system (1) in one spatial dimension with periodic boundary conditions,

$$\begin{aligned} \tau_\theta\dot{\theta}_k &= l^2\left(\frac{\theta_{k-1} - 2\theta_k + \theta_{k+1}}{\delta^2}\right) - \theta_k^3 + \theta_k + \eta_k, \\ \tau_\eta\dot{\eta}_k &= L^2\left(\frac{\eta_{k-1} - 2\eta_k + \eta_{k+1}}{\delta^2}\right) - \eta_k - \theta_k + C, \end{aligned} \tag{16}$$

where the overdot denotes differentiation with respect to time, δ is the distance between the discretized points along the x-axis where we are evaluating θ_k and η_k, and the indices k are taken mod N, where $2N$ is the total number of ODEs. (The spatially discretized version of the cubic nonlinearity model satisfies dissipativity bounds analogous to those obtained in the PDE case. Since the necessary local Lipschitz condition is satisfied, and the dissipativity bounds preclude finite escape times, existence and uniqueness of solutions for the spatially discretized system of ODEs is easily established [33].)

As for the PDE system, we can write this discretized system as a gradient system with respect to an indefinite metric: let

$$\tilde{V} = \frac{l^2}{\delta^2}\left(\sum_k \theta_k^2 - \sum_k \theta_k\theta_{k+1}\right) + \frac{1}{4}\sum_k \theta_k^4 - \frac{1}{2}\sum_k \theta_k^2 - \sum_k \theta_k\eta_k,$$
$$- \frac{L^2}{\delta^2}\left(\sum_k \eta_k^2 - \sum_k \eta_k\eta_{k+1}\right) - \frac{1}{2}\sum_k \eta_k^2 + C\sum_k \eta_k, \tag{17}$$

so that

$$\begin{aligned}\frac{d\tilde{V}}{dt} &= \sum_k \frac{\partial \tilde{V}}{\partial \theta_k}\dot{\theta}_k + \sum_k \frac{\partial \tilde{V}}{\partial \eta_k}\dot{\eta}_k \\ &= -\sum_k \left[\tau_\theta(\dot{\theta}_k)^2 - \tau_\eta(\dot{\eta}_k)^2\right] \\ &= -[\dot{\theta}^T \ \dot{\eta}^T]\begin{bmatrix}\tau_\theta I & 0 \\ 0 & -\tau_\eta I\end{bmatrix}\begin{bmatrix}\dot{\theta} \\ \dot{\eta}\end{bmatrix},\end{aligned} \tag{18}$$

where $\theta = (\theta_1, \ldots, \theta_N)$, $\eta = (\eta_1, \ldots, \eta_N)$, and I denotes the $N \times N$ identity matrix. As before, we can equivalently express this as

$$-\tilde{J}\begin{bmatrix}\dot{\theta} \\ \dot{\eta}\end{bmatrix} = \nabla\tilde{V}, \tag{19}$$

so that

$$\frac{d\tilde{V}}{dt} = [\dot{\theta}^T \ \dot{\eta}^T]\nabla\tilde{V} = -[\dot{\theta}^T \ \dot{\eta}^T]\tilde{J}\begin{bmatrix}\dot{\theta} \\ \dot{\eta}\end{bmatrix}, \tag{20}$$

where

$$\tilde{J} = \begin{bmatrix}\tau_\theta I & 0 \\ 0 & -\tau_\eta I\end{bmatrix}. \tag{21}$$

The technique of Brayton and Moser involves first computing $D^2\tilde{V}$, which looks like

$$D^2\tilde{V} = \begin{bmatrix} \frac{\partial^2\tilde{V}}{\partial\theta_1^2} & \cdots & \frac{\partial^2\tilde{V}}{\partial\theta_1\partial\theta_N} & \frac{\partial^2\tilde{V}}{\partial\theta_1\partial\eta_1} & \cdots & \frac{\partial^2\tilde{V}}{\partial\theta_1\partial\eta_N} \\ \vdots & & \vdots & \vdots & & \vdots \\ \frac{\partial^2\tilde{V}}{\partial\theta_1\partial\theta_N} & \cdots & \frac{\partial^2\tilde{V}}{\partial\theta_N^2} & \frac{\partial^2\tilde{V}}{\partial\theta_N\partial\eta_1} & \cdots & \frac{\partial^2\tilde{V}}{\partial\theta_N\partial\eta_N} \\ \frac{\partial^2\tilde{V}}{\partial\theta_1\partial\eta_1} & \cdots & \frac{\partial^2\tilde{V}}{\partial\theta_N\partial\eta_1} & \frac{\partial^2\tilde{V}}{\partial\eta_1^2} & \cdots & \frac{\partial^2\tilde{V}}{\partial\theta_1\partial\eta_N} \\ \vdots & & \vdots & \vdots & & \vdots \\ \frac{\partial^2\tilde{V}}{\partial\theta_1\partial\eta_N} & \cdots & \frac{\partial^2\tilde{V}}{\partial\theta_N\partial\eta_N} & \frac{\partial^2\tilde{V}}{\partial\eta_1\partial\eta_N} & \cdots & \frac{\partial^2\tilde{V}}{\partial\eta_N^2} \end{bmatrix}$$
$$= \begin{bmatrix}P & -I \\ -I & Q\end{bmatrix}, \tag{22}$$

where each block is $N \times N$. It turns out not to be necessary to compute P, but it is necessary to write down Q and show that Q is invertible. A simple calculation gives

$$Q = -\left(I + \frac{L^2}{\delta^2} R\right), \tag{23}$$

where

$$R = \begin{bmatrix} 2 & -1 & 0 & \cdots & 0 & -1 \\ -1 & 2 & -1 & 0 & \cdots & 0 \\ 0 & -1 & 2 & -1 & & \vdots \\ \vdots & 0 & & \ddots & & 0 \\ 0 & \vdots & & & 2 & -1 \\ -1 & 0 & \cdots & 0 & -1 & 2 \end{bmatrix}. \tag{24}$$

R is easily seen to be positive semidefinite. Therefore, Q is negative definite, and hence invertible. Then defining

$$M = \begin{bmatrix} 0 & 0 \\ 0 & -2Q^{-1} \end{bmatrix}, \tag{25}$$

we can define

$$\begin{aligned} J &= \tilde{J} + (D^2\tilde{V})M\tilde{J} \\ &= \begin{bmatrix} \tau_\theta I & 0 \\ 0 & -\tau_\eta I \end{bmatrix} + \begin{bmatrix} P & -I \\ -I & Q \end{bmatrix} \begin{bmatrix} 0 & 0 \\ 0 & -2Q^{-1} \end{bmatrix} \begin{bmatrix} \tau_\theta I & 0 \\ 0 & -\tau_\eta I \end{bmatrix} \\ &= \begin{bmatrix} \tau_\theta I & 0 \\ 0 & -\tau_\eta I \end{bmatrix} + \begin{bmatrix} 0 & -2\tau_\eta Q^{-1} \\ 0 & 2\tau_\eta I \end{bmatrix} \\ &= \begin{bmatrix} \tau_\theta I & -2\tau_\eta Q^{-1} \\ 0 & \tau_\eta I \end{bmatrix}. \end{aligned} \tag{26}$$

Corresponding to this J, there is a

$$V = \tilde{V} + \frac{1}{2}(\nabla\tilde{V})^T M \nabla\tilde{V}, \tag{27}$$

such that

$$-J \begin{bmatrix} \dot{\theta} \\ \dot{\eta} \end{bmatrix} = \nabla V. \tag{28}$$

To see this, simply take the gradient of V:

$$\begin{aligned} \nabla V &= \nabla\tilde{V} + (D^2\tilde{V})M\nabla\tilde{V} \\ &= -(\tilde{J} + (D^2\tilde{V})M\tilde{J}) \begin{bmatrix} \dot{\theta} \\ \dot{\eta} \end{bmatrix} \\ &= -J \begin{bmatrix} \dot{\theta} \\ \dot{\eta} \end{bmatrix}. \end{aligned} \tag{29}$$

If J were symmetric, there would be a well-defined metric, and the dynamics would be gradient dynamics. However, J is not symmetric. But if (the symmetric part of) J is positive definite, V will still be decreasing along trajectories. If we can further show that V is radially unbounded and $\dot{V} = 0$ if and only if $\dot{\theta} = \dot{\eta} = 0$, we will be able to conclude that the trajectories of the system converge to the set of equilibrium points.

As for the positive definiteness of (the symmetric part of) J, we have

$$\begin{aligned}
&[\dot{\theta}^T \quad \dot{\eta}^T] \begin{bmatrix} \tau_\theta I & -2\tau_\eta Q^{-1} \\ 0 & \tau_\eta I \end{bmatrix} \begin{bmatrix} \dot{\theta} \\ \dot{\eta} \end{bmatrix} \\
&\quad = \tau_\theta |\dot{\theta}|^2 + \tau_\eta |\dot{\eta}|^2 - 2\tau_\eta \dot{\theta}^T Q^{-1} \dot{\eta} \\
&\quad = \left| \sqrt{\tau_\theta}\dot{\theta} - \frac{1}{\sqrt{\alpha}} Q^{-1}(\sqrt{\tau_\eta}\dot{\eta}) \right|^2 + \left| \sqrt{\tau_\eta}\dot{\eta} \right|^2 - \frac{1}{\alpha} \left| Q^{-1}(\sqrt{\tau_\eta}\dot{\eta}) \right|^2, \qquad (30)
\end{aligned}$$

and if

$$\frac{1}{\sqrt{\alpha}} ||Q^{-1}|| < 1, \qquad (31)$$

then we see that (the symmetric part of) J is positive definite. Furthermore, we can calculate $||Q^{-1}|| = 1$ by finding the smallest singular value of $-Q$, and then inverting it. Observing that for $||\mathbf{z}|| = 1$ we have

$$\mathbf{z}^T(-Q)\mathbf{z} = \mathbf{z}^T \left(I + \frac{L^2}{\delta^2} R \right) \mathbf{z} = 1 + \frac{L^2}{\delta^2} \mathbf{z}^T R \mathbf{z}, \qquad (32)$$

and in light of the fact that R is positive semidefinite and $\mathbf{z}$ can be chosen such that $\mathbf{z}^T R \mathbf{z} = 0$, it is clear that the smallest singular value of $-Q$ is 1. Hence, $||Q^{-1}|| = 1$, and we arrive at the condition that (the symmetric part of) J is positive definite if

$$\alpha > 1. \qquad (33)$$

Because

$$\dot{V} = -[\dot{\theta}^T \quad \dot{\eta}^T] J \begin{bmatrix} \dot{\theta} \\ \dot{\eta} \end{bmatrix}, \qquad (34)$$

we also see that if J is positive definite, then $\dot{V} \leq 0$, and $\dot{V} = 0$ if and only if $\dot{\theta} = \dot{\eta} = 0$.

Next, we need to compute V and determine that it is radially unbounded. We define

$$\nabla \tilde{V} = \begin{bmatrix} \nabla_\theta \tilde{V} \\ \nabla_\eta \tilde{V} \end{bmatrix}, \qquad (35)$$

so that $\nabla_\theta \tilde{V}$ represents the gradient of $\tilde{V}$ with respect to the θ_k only, and $\nabla_\eta \tilde{V}$ represents the gradient of $\tilde{V}$ with respect to the η_k only. Then from (27) and (25) we can express V as

$$V = \tilde{V} - (\nabla_\eta \tilde{V})^T Q^{-1} \nabla_\eta \tilde{V}. \qquad (36)$$

Furthermore, we can directly calculate that

$$\frac{\partial \tilde{V}}{\partial \eta_k} = \left(-2\frac{L^2}{\delta^2} - 1\right)\eta_k + \frac{L^2}{\delta^2}\eta_{k-1} + \frac{L^2}{\delta^2}\eta_{k+1} - \theta_k + C, \tag{37}$$

and hence that

$$\nabla_\eta \tilde{V} = Q\eta - \theta + C\begin{bmatrix} 1 \\ 1 \\ \vdots \\ 1 \end{bmatrix}. \tag{38}$$

We thus compute

$$\begin{aligned} V = {} & \frac{l^2}{\delta^2}\left(\sum_k \theta_k^2 - \sum_k \theta_k\theta_{k+1}\right) + \frac{1}{4}\sum_k \theta_k^4 - \frac{1}{2}\sum_k \theta_k^2 \\ & + \frac{L^2}{\delta^2}\left(\sum_k \eta_k^2 - \sum_k \eta_k\eta_{k+1}\right) + \frac{1}{2}\sum_k \eta_k^2 - C\sum_k \eta_k \\ & + \sum_k \theta_k\eta_k - (\theta - C\chi)^T Q^{-1}(\theta - C\chi), \end{aligned} \tag{39}$$

where $\chi = [1 \;\; 1 \;\; \cdots \;\; 1]^T$. It can be shown that V is radially unbounded, meaning $V \to \infty$ whenever $|\theta_k| \to \infty$ or $|\eta_k| \to \infty$, for any k. We thus arrive at the conclusion that for the discretized one-dimensional system with periodic boundary conditions, regardless of the fineness of the discretization (N and δ), as long as $\alpha > 1$, we can find a radially unbounded Lyapunov function V such that $\dot{V} \leq 0$, and with $\dot{V} = 0$ if and only if $\dot{\theta} = \dot{\eta} = 0$. We can therefore conclude that all trajectories must converge to the set of equilibrium points, provided $\alpha > 1$. If we have Dirichlet or Neumann boundary conditions, similar conclusions can be reached [24].

For discretized systems in more than one spatial dimension, the results for the one-dimensional case carry over, as long as the domain Ω is rectangular. For example, in two spatial dimensions with periodic boundary conditions, the simplest discretization would be

$$\begin{aligned} \tau_\theta \dot{\theta}_{jk} &= l^2\left(\frac{\theta_{j(k+1)} + \theta_{j(k-1)} + \theta_{(j+1)k} + \theta_{(j-1)k} - 4\theta_{jk}}{\delta^2}\right) - \theta_{jk}^3 + \theta_{jk} + \eta_{jk}, \\ \tau_\eta \dot{\eta}_{jk} &= L^2\left(\frac{\eta_{j(k+1)} + \eta_{j(k-1)} + \eta_{(j+1)k} + \eta_{(j-1)k} - 4\eta_{jk}}{\delta^2}\right) \\ & \quad - \eta_{jk} - \theta_{jk} + C. \end{aligned} \tag{40}$$

All the same calculations can be performed on this system as in the one-dimensional case, and the conclusions are the same.

4.3. Convergence Result for the Spatially Discretized Cubic Nonlinearity Model

With the Lyapunov function V given by equation (39) for the spatially discretized system, we can prove a rigorous convergence result using the following theorem, (see [33]):

Theorem 1 (LaSalle's Invariance Principle). *Consider the system $\dot{v} = f(v)$. Let Σ be a compact set and suppose the solution $v(t)$ starting in Σ stays in Σ for all $t > 0$. Let $V\colon \Sigma \to \mathbb{R}$ be a continuous function such that $V(v(t))$ is a monotone nonincreasing function of t. Let E be the set of all points in Ω where $\dot{V}(v)$ exists and equals zero. Let M be the largest positively invariant set in E. Then $v(t)$ approaches M as $t \to \infty$.*

Our preliminary convergence result is the following:

Theorem 2. *Assume $\alpha = \tau_\theta/\tau_\eta > 1$. Then every trajectory of the spatially discretized system* (16) *(corresponding to periodic, Neumann, or Dirichlet boundary conditions for the original PDE system) converges to the set of equilibria of the dynamics.*

Proof. The existence of the compact invariant set Σ is guaranteed by the radial unboundedness of V. Also, $E = M$ is simply the set of equilibria of the dynamics, due to equation (34). Applying LaSalle's invariance principle completes the proof. □

To prove convergence of each trajectory to an equilibrium, we need to use the fact that V is analytic. The proof is essentially identical to the proof of convergence for gradient flows with analytic cost functions [34], [35]. Related techniques and methods also appear in [36]. The proof is based on a result of Lojasiewicz [34], [35], [37]:

Lemma (Lojasiewicz). *Let $f\colon \mathbb{R}^n \to \mathbb{R}$ be a real analytic function, and let $v^* \in \mathbb{R}^n$ be a critical point. Then there exists a neighborhood $U \subset \mathbb{R}^n$ and a real number $\mu \in (0, 1)$ such that*

$$|f(v) - f(v^*)|^\mu \leq |\nabla f(v)|, \qquad \forall v \in U. \tag{41}$$

Proof. See [34], [35], [37]. □

Theorem 3. *Assume that V is analytic, J is positive definite (but not necessarily symmetric), $\dot{v} = f(v) = -J^{-1}\nabla V$, and the hypotheses of Theorem* 1 *are satisfied. Suppose also that $\dot{V} = -(\nabla V)^T J^{-1} \nabla V$. Then $\lim_{t\to\infty} v(t) = v^*$ for some equilibrium point v^*.*

Proof. Essentially as given in [34], [35]. See Appendix. □

Theorem 4. *Assume $\alpha = \tau_\theta/\tau_\eta > 1$. Then every trajectory of the spatially discretized system* (16) *(corresponding to periodic, Neumann, or Dirichlet boundary conditions for the original PDE system) converges to an equilibrium.*

Proof. Follows directly from Theorem 3 and Theorem 2. □

4.4. Lyapunov Functional Derivation for the Cubic Nonlinearity Model

We can generalize the technique of Brayton and Moser to the infinite-dimensional setting and use it to find a Lyapunov functional for the basic cubic nonlinearity model.

The first step is to calculate the second derivative of the energy functional $\tilde{V}$. We have

$$\tilde{V}\colon X \to \mathbb{R}, \tag{42}$$

where X represents the space in which the (θ, η) lie. At each $\mathbf{p} \in X$, there is a derivative map,

$$\begin{aligned} D\tilde{V}_{\mathbf{p}}\colon X &\to \mathbb{R} \\ \mathbf{u} &\mapsto D\tilde{V}_{\mathbf{p}} \cdot \mathbf{u} = \frac{d}{d\epsilon}\tilde{V}(\mathbf{p} + \epsilon\mathbf{u})\Big|_{\epsilon=0}, \end{aligned} \tag{43}$$

which corresponds to the first variation of $\tilde{V}$ evaluated at a particular (θ, η). By $\nabla\tilde{V}$, we mean

$$\nabla\tilde{V} = \begin{bmatrix} -l^2\Delta\theta + \theta^3 - \theta - \eta \\ L^2\Delta\eta - \eta - \theta + C \end{bmatrix}, \tag{44}$$

for then

$$D\tilde{V}_{(\theta,\eta)} \cdot \begin{bmatrix} \delta\theta \\ \delta\eta \end{bmatrix} = \int_\Omega \nabla\tilde{V} \cdot \begin{bmatrix} \delta\theta \\ \delta\eta \end{bmatrix} d\mathbf{x}, \tag{45}$$

where $\int_\Omega \mathbf{u} \cdot \mathbf{v}\, d\mathbf{x}$ is our inner product. We can then define the second-derivative map at a point $\mathbf{p} \in X$ as

$$\begin{aligned} D^2\tilde{V}_{\mathbf{p}}\colon X \times X &\to \mathbb{R} \\ (\mathbf{u}, \mathbf{v}) &\mapsto \frac{d^2}{d\epsilon d\xi}\tilde{V}(\mathbf{p} + \epsilon\mathbf{u} + \xi\mathbf{v})\Big|_{\epsilon=0,\xi=0}. \end{aligned} \tag{46}$$

We can define the second-derivative matrix $D^2\tilde{V}$ by

$$D^2\tilde{V}_{(\theta,\eta)} \cdot \left(\begin{bmatrix} \delta\theta_1 \\ \delta\eta_1 \end{bmatrix}, \begin{bmatrix} \delta\theta_2 \\ \delta\eta_2 \end{bmatrix} \right) = \int_\Omega [\delta\theta_1 \;\; \delta\eta_1]\, D^2\tilde{V} \begin{bmatrix} \delta\theta_2 \\ \delta\eta_2 \end{bmatrix} d\mathbf{x}. \tag{47}$$

The second-derivative matrix $D^2\tilde{V}$ is computed to be

$$D^2\tilde{V} = \begin{bmatrix} (3\theta^2 - 1 - l^2\Delta) & -1 \\ -1 & (-1 + L^2\Delta) \end{bmatrix}. \tag{48}$$

We thus see that the quantity that plays the role of the matrix Q in the discretized system is the operator $(-1 + L^2\Delta)$. Therefore, we need to address the issue of finding an inverse for $(-1 + L^2\Delta)$.

Suppose that we have periodic boundary conditions. Since the functions $(\delta\theta, \delta\eta)$ we are working with are in $L^2(\Omega)$, their Fourier series are well-defined (in the distributional sense):

$$\begin{aligned} u(\mathbf{x}) &= \sum_{\mathbf{k}} u_{\mathbf{k}} e^{i\mathbf{k}\cdot\mathbf{x}}, \\ u_{\mathbf{k}} &= \frac{1}{|\Omega|}\int_{\Omega} u(\mathbf{x}) e^{-i\mathbf{k}\cdot\mathbf{x}} d\mathbf{x}, \\ u(\mathbf{x}) &\in L^2(\Omega), \quad \sum_{\mathbf{k}} |u_{\mathbf{k}}|^2 < \infty. \end{aligned} \tag{49}$$

(Here we are thinking of $\mathbf{k}$ as a vector containing indices which are not necessarily integer. For example, in the one-dimensional case, we would have $k = 2\pi m/\mathcal{L}$ where m is an integer and $\mathcal{L} = |\Omega|$ is the length of the interval Ω.) Then

$$(-1 + L^2\Delta)u(\mathbf{x}) = -\sum_{\mathbf{k}} (1 + L^2|\mathbf{k}|^2) u_{\mathbf{k}} e^{i\mathbf{k}\cdot\mathbf{x}}, \tag{50}$$

so the inverse operator for $(-1 + L^2\Delta)$ has the form

$$(-1 + L^2\Delta)^{-1} v(\mathbf{x}) = w(\mathbf{x}) * v(\mathbf{x}) = \int_{\Omega} w(\mathbf{x} - \mathbf{y}) v(\mathbf{y}) d\mathbf{y}, \tag{51}$$

where $w(\mathbf{x})$ can be represented as

$$w(\mathbf{x}) = \sum_{\mathbf{k}} \frac{-1}{1 + L^2|\mathbf{k}|^2} e^{i\mathbf{k}\cdot\mathbf{x}}. \tag{52}$$

Before we can conclude that we have an appropriate inverse, however, we need to verify, since $(-1 + L^2\Delta)$ takes functions in $H^2(\Omega)$ to $L^2(\Omega)$, that $w(\mathbf{x}) * \cdot$ takes functions in $L^2(\Omega)$ to $H^2(\Omega)$. But this is in fact the case, since an equivalent norm to the $H^2(\Omega)$ norm is [32]

$$\|u\|_2 = \left(\sum_{\mathbf{k}} |u_{\mathbf{k}}|^2 \left(1 + |\mathbf{k}|^2\right)^2 \right)^{1/2}. \tag{53}$$

Thus, from the form of $w(\mathbf{x})*\cdot$, it is clear that $w(\mathbf{x})*v(\mathbf{x}) \in H^2(\Omega)$ if $v(\mathbf{x}) \in L^2(\Omega)$. Thus, we have verified (at least for periodic boundary conditions) that $(-1+L^2\Delta)^{-1}$: $L^2(\Omega) \to H^2(\Omega)$ is a well-defined operator.

Proceeding by analogy with the spatially discretized case, we can compute

$$V = \tilde{V} - (\nabla_\eta \tilde{V}, (-1 + L^2\Delta)^{-1} \nabla_\eta \tilde{V}), \tag{54}$$

where

$$\nabla_\eta \tilde{V} = L^2\Delta\eta - \theta - \eta + C = (-1 + L^2\Delta)\eta - \theta + C. \tag{55}$$

Calculating

$$
\begin{aligned}
&(\nabla_\eta \tilde{V}, (-1+L^2\Delta)^{-1}\nabla_\eta \tilde{V}) \\
&\quad = \int_\Omega [(-1+L^2\Delta)\eta - \theta + C][(-1+L^2\Delta)^{-1}[(-1+L^2\Delta)\eta - \theta + C]]d\mathbf{x} \\
&\quad = \int_\Omega [-L^2|\nabla\eta|^2 - \eta^2 - 2\theta\eta + 2C\eta \\
&\qquad - (-\theta + C)[(-1+L^2\Delta)^{-1}(-\theta + C)]]d\mathbf{x}, \qquad (56)
\end{aligned}
$$

where integration by parts has been used (with the assumption of periodic boundary conditions), we finally obtain

$$
\begin{aligned}
V = \int_\Omega \Big[&\frac{l^2}{2}|\nabla\theta|^2 + \frac{1}{4}\theta^4 - \frac{1}{2}\theta^2 + \frac{L^2}{2}|\nabla\eta|^2 + \frac{1}{2}\eta^2 - C\eta + \theta\eta \\
&- (\theta - C)\,[(-1+L^2\Delta)^{-1}(\theta - C)]\Big] d\mathbf{x}. \qquad (57)
\end{aligned}
$$

From this expression for V, it is apparent that V is radially unbounded (i.e., $V \to \infty$ whenever any of $||\theta||_{L^2(\Omega)}$, $||\eta||_{L^2(\Omega)}$, $||\nabla\theta||_{L^2(\Omega)}$, or $||\nabla\eta||_{L^2(\Omega)}$ goes to infinity).

It now remains to determine ∇V, so that we can check whether (or under what conditions) $\dot{V} \leq 0$, with $\dot{V} = 0$ only at equilibria. The only term of V for which we have not yet computed the first variation is the $(-\theta + C)[(-1+L^2\Delta)^{-1}(-\theta + C)]$ term. Using the representation $(-1+L^2\Delta)^{-1}\cdot = w * \cdot$, we compute

$$
\begin{aligned}
&\frac{\delta}{\delta\theta}\left[\int_\Omega (-\theta + C)[(-1+L^2\Delta)^{-1}(-\theta + C)]d\mathbf{x}\right]\cdot u \\
&\qquad = \int_\Omega 2[(-1+L^2\Delta)^{-1}(-\theta + C)]u\, d\mathbf{x}. \qquad (58)
\end{aligned}
$$

Therefore, we have

$$
\begin{aligned}
\nabla_\theta V &= -l^2\Delta\theta + \theta^3 - \theta + \eta + 2(-1+L^2\Delta)^{-1}(-\theta + C) \\
&= -\tau_\theta \frac{\partial\theta}{\partial t} + 2[\eta + (-1+L^2\Delta)^{-1}(-\theta + C)], \\
\nabla_\eta V &= -L^2\Delta\eta + \eta + \theta - C = -\tau_\eta \frac{\partial\eta}{\partial t}. \qquad (59)
\end{aligned}
$$

Observing that

$$
\begin{aligned}
2\tau_\eta(-1+L^2\Delta)^{-1}\frac{\partial\eta}{\partial t} &= 2(-1+L^2\Delta)^{-1}(L^2\Delta\eta - \eta - \theta + C) \\
&= 2[\eta + (-1+L^2\Delta)^{-1}(-\theta + C)], \qquad (60)
\end{aligned}
$$

we conclude that ∇V can be expressed as

$$
\nabla V = -\begin{bmatrix} \tau_\theta & -2\tau_\eta(-1+L^2\Delta)^{-1} \\ 0 & \tau_\eta \end{bmatrix}\begin{bmatrix} \partial\theta/\partial t \\ \partial\eta/\partial t \end{bmatrix}. \qquad (61)
$$

Therefore,

$$\dot{V} = -\int_\Omega \begin{bmatrix} \frac{\partial\theta}{\partial t} & \frac{\partial\eta}{\partial t} \end{bmatrix} \begin{bmatrix} \tau_\theta & -2\tau_\eta(-1+L^2\Delta)^{-1} \\ 0 & \tau_\eta \end{bmatrix} \begin{bmatrix} \partial\theta/\partial t \\ \partial\eta/\partial t \end{bmatrix} d\mathbf{x}$$

$$= -\int_\Omega \left[\left(\sqrt{\tau_\theta}\frac{\partial\theta}{\partial t} - \frac{1}{\sqrt{\alpha}}(-1+L^2\Delta)^{-1}\left(\sqrt{\tau_\eta}\frac{\partial\eta}{\partial t}\right)\right)^2 + \left(\sqrt{\tau_\eta}\frac{\partial\eta}{\partial t}\right)^2 \right.$$

$$\left. - \frac{1}{\alpha}\left((-1+L^2\Delta)^{-1}\left(\sqrt{\tau_\eta}\frac{\partial\eta}{\partial t}\right)\right)^2 \right] d\mathbf{x}. \tag{62}$$

Thus, the sufficient condition for $\dot{V} \leq 0$ is

$$\frac{1}{\sqrt{\alpha}}||(-1+L^2\Delta)^{-1}|| < 1, \tag{63}$$

where we are using the operator norm for $||(-1+L^2\Delta)^{-1}||$ defined by

$$||(-1+L^2\Delta)^{-1}|| = \sup_{u\in U} ||(-1+L^2\Delta)^{-1}u||_{L^2(\Omega)}, \qquad U = \{u\colon\ ||u||_{L^2(\Omega)} = 1\}. \tag{64}$$

Since the eigenvalues of $(1-L^2\Delta)$ are $(1+L^2|\mathbf{k}|^2)$, and the eigenvalues of $(1-L^2\Delta)^{-1}$ are $1/(1+L^2|\mathbf{k}|^2)$, with $\mathbf{k}=\mathbf{0}$ an admissible eigenvalue, it follows as in the discretized case that $||(-1+L^2\Delta)^{-1}|| = 1$, and we arrive at the same sufficient condition for $\dot{V} \leq 0$, namely,

$$\alpha > 1. \tag{65}$$

Thus, for periodic boundary conditions, we see that in analogy with the spatially discretized case, if $\alpha > 1$ then there is a radially unbounded Lyapunov functional V such that $\dot{V} \leq 0$, and with $\dot{V} = 0$ only at equilibria of the dynamics.

For Dirichlet or Neumann boundary conditions, we need to assume that the boundary of Ω is C^2 (so that we have the necessary second-derivative bounds required for calculating the variations of $\tilde{V}$ and V), and we need to use Fourier transform techniques instead of Fourier series techniques. Similar results are then obtained [24].

5. Related Systems

Various systems related to the cubic nonlinearity activator inhibitor system (1) can be analyzed using the techniques described above. For example, symmetric long-range coupling can be added to the activator equation of system (1), or the cubic nonlinearity can be replaced by a bounded nonlinearity [24]. One related system which is interesting in its own right as well as useful for further exploring the properties of system (1) is the complex activator-inhibitor equation obtained by taking θ and η in equation (1) to be complex, and replacing θ^3 by $|\theta|^2\theta$. Another interesting system, an active transmission line, is obtained by using gradient coupling terms instead of (or in addition to) the linear, zeroth-order coupling terms.

5.1. *Complex Activator-Inhibitor Equation*

The complex activator-inhibitor equation is

$$\begin{aligned}\tau_\theta \frac{\partial \theta}{\partial t} &= l^2 \Delta \theta - |\theta|^2 \theta + \theta + \eta, \\ \tau_\eta \frac{\partial \eta}{\partial t} &= L^2 \Delta \eta - \eta - \theta + C,\end{aligned} \tag{66}$$

where $\theta(\mathbf{x}, t)$, $\eta(\mathbf{x}, t)$, and the bifurcation parameter C are complex, while τ_θ, τ_η, l, and L are positive real constants. The complex activator-inhibitor equation can be used, under suitable hypotheses, to model the amplitude and phase evolution in the continuum limit of a network of coupled van der Pol oscillators (represented by θ), coupled to a network of resonant circuits (represented by η), with an external oscillating input (represented by C). The resonant frequencies of the van der Pol oscillators and the resonant circuits are assumed to be identical, and also equal to the frequency of the external input C.

System (66) can be rewritten as a coupled system of four real equations, which look like two real activator-inhibitor systems nonlinearly coupled to each other through their activator equations. As a result, the mathematical analysis for system (1) easily carries over to system (66) [24]. When $\alpha > 1$, system (66) possesses a Lyapunov functional

$$\begin{aligned}V = \int_\Omega \Big[&\frac{l^2}{2}|\nabla\theta|^2 + \frac{1}{4}|\theta|^4 - \frac{1}{2}|\theta|^2 + \frac{L^2}{2}|\nabla\eta|^2 + \frac{1}{2}|\eta|^2 - \mathrm{Re}\{\overline{C}\eta\} + \mathrm{Re}\{\overline{\theta}\eta\} \\ &- (\overline{\theta} - \overline{C})\left[(-1 + L^2\Delta)^{-1}(\theta - C)\right] \Big] d\mathbf{x},\end{aligned} \tag{67}$$

where the overbar denotes complex conjugation. The time derivative of V is then found to be

$$\begin{aligned}\dot{V} = -\int_\Omega &\begin{bmatrix} \partial\theta_R/\partial t \\ \partial\theta_I/\partial t \\ \partial\eta_R/\partial t \\ \partial\eta_I/\partial t \end{bmatrix}^T \begin{bmatrix} \tau_\theta & 0 & -2\tau_\eta(-1 + L^2\Delta)^{-1} & 0 \\ 0 & \tau_\theta & 0 & -2\tau_\eta(-1 + L^2\Delta)^{-1} \\ 0 & 0 & \tau_\eta & 0 \\ 0 & 0 & 0 & \tau_\eta \end{bmatrix} \\ &\times \begin{bmatrix} \partial\theta_R/\partial t \\ \partial\theta_I/\partial t \\ \partial\eta_R/\partial t \\ \partial\eta_I/\partial t \end{bmatrix} d\mathbf{x},\end{aligned} \tag{68}$$

where θ_R, θ_I, η_R, and η_I are the real and imaginary parts of θ and η. When $\alpha = \tau_\theta/\tau_\eta > 1$, we can conclude that $\dot{V} \leq 0$, and $\dot{V} = 0$ only at equilibria [2], [24]. Since V is radially unbounded, it serves as a Lyapunov functional provided $\alpha > 1$.

The equilibria for the complex activator inhibitor system (66) differ somewhat from the equilibria of system (1). For example, system (66) does not have the localized spike equilibria that system (1) has. If $|C|$ is sufficiently large for system (66), a spatially uniform equilibrium is stable. In the coupled oscillator context, large $|C|$ corresponds to driving the oscillators with a sufficiently large-amplitude input signal that all of the oscillators phase-lock to the input signal. If $C = 0$ (which in the coupled oscillator

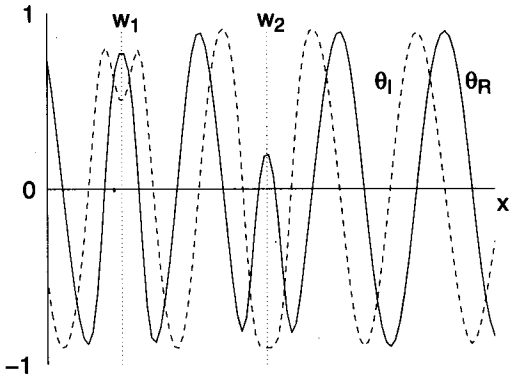

Fig. 9. A one-dimensional equilibrium for the complex activator-inhibitor equation having two domain walls (indicated by w_1 and w_2).

context corresponds to no external input), then an equilibrium consisting of parallel rolls is stable, and the real and imaginary parts of θ and η are sinusoidal along the direction perpendicular to the rolls. In the intermediate case between $C = 0$ and $|C|$ large, higher spatial harmonics (besides the fundamental frequency when $C = 0$) are introduced into the equilibrium phase pattern.

Just as patterns for system (1) could be irregular, patterns for system (66) need not be ideal. In particular, domain walls can form between left-handed and right-handed versions of the same spatially periodic pattern, as illustrated in Figure 9 for a single space dimension.

The complex activator-inhibitor equation may be of interest in its own right for control of large arrays of coupled oscillators, with potential applications being quasi-optical power combining, phased-array antennas, or control of osillatory MEMS actuators [2]. Another key feature of the complex activator-inhibitor equation is that a modal analysis is straightforward, and the results can be applied to system (1). To perform the modal analysis, we assume a fundamental wave number corresponding to the wave number of an ideal pattern solution, and take this as the lowest-order (nonzero) mode in our modal expansion of the dynamics. We first rescale the dynamics by the fundamental wave number which we take here to be $\sqrt{1-\beta}/\sqrt{lL}$, since this is the wave number of the lowest-energy ideal pattern equilibrium when $C = 0$ (i.e., lowest energy with respect to our Lyapunov functional). Next, we obtain the dynamical equations for the modal coefficients. Then we present a Lyapunov function for any finite number of modes. Finally, we present a bound on the higher-order modes so that we can justify retaining only the lower-order modes to obtain a good approximation of the equilibrium of interest.

The rescaled dynamics are

$$\begin{aligned} \tau_\theta \frac{\partial \theta}{\partial t} &= \beta(1-\beta)\frac{\partial^2 \theta}{\partial x^2} - |\theta|^2\theta + \theta + \eta, \\ \tau_\eta \frac{\partial \eta}{\partial t} &= \frac{1-\beta}{\beta}\frac{\partial^2 \eta}{\partial x^2} - \eta - \theta + C. \end{aligned} \tag{69}$$

Plugging in the Fourier series expansions

$$\theta = \sum_k \theta_k e^{ikx}, \qquad \eta = \sum_k \eta_k e^{ikx}, \tag{70}$$

where because of the rescaling, k takes integer values, gives

$$\begin{aligned}
\tau_\theta \dot{\theta}_m &= (1 - m^2\beta(1-\beta))\theta_m \\
&\quad - \Bigg[|\theta_m|^2\theta_m + 2\sum_{j\neq m} |\theta_j|^2\theta_m + \sum_{k\neq m} \overline{\theta}_{2k-m}\theta_k^2 \\
&\qquad + \sum_j \sum_{k\neq j,m,(m+j)/2} \overline{\theta}_j \theta_k \theta_{m+j-k} \Bigg] + \eta_m, \\
\tau_\eta \dot{\eta}_m &= -\left(1 + m^2 \frac{1-\beta}{\beta}\right)\eta_m - \theta_m + C\delta_{m0},
\end{aligned} \tag{71}$$

where $\delta_{jk} = 1$ for $j = k$ and $\delta_{jk} = 0$ otherwise. Let

$$\begin{aligned}
V &= -\frac{1}{2}\sum_m (1 - m^2\beta(1-\beta))|\theta_m|^2 + \frac{1}{4}\sum_m |\theta_m|^4 + \frac{1}{2}\sum_m \sum_{j\neq m} |\theta_j|^2|\theta_m|^2 \\
&\quad + \mathrm{Re}\left\{\frac{1}{2}\sum_m \sum_{k\neq m} \overline{\theta}_{2k-m}\theta_k^2 \overline{\theta}_m\right\} + \mathrm{Re}\left\{\frac{1}{4}\sum_m \sum_{j\neq m} \sum_{k\neq j,m,(m+j)/2} \overline{\theta}_j \theta_k \theta_{m+j-k}\overline{\theta}_m\right\} \\
&\quad + \frac{1}{2}\sum_m \left(1 + m^2\frac{1-\beta}{\beta}\right)|\eta_m|^2 - \mathrm{Re}\{C\overline{\eta}_0\} + \sum_m \mathrm{Re}\{\overline{\theta_m}\eta_m\} \\
&\quad + \sum_m \left(1 + m^2\frac{1-\beta}{\beta}\right)^{-1} |\theta_m - C\delta_{m0}|^2.
\end{aligned} \tag{72}$$

Then the function V given above, appropriately truncated, is a radially unbounded Lyapunov function for the dynamics given by equation (71) for any finite number of modes (as can be proved by direct differentiation). We find that if $\alpha = \tau_\theta/\tau_\eta > 1$, then $\dot{V} \leq 0$, with $\dot{V} = 0$ only for equilibria (for any finite number of modes).

We can obtain the following bound for the error in approximating the exact equilibrium solution θ with its finite modal approximation $\sum_{k=-N}^{N} \theta_k e^{ikx}$:

$$\left|\theta - \sum_{k=-N}^{N} \theta_k e^{ikx}\right| \leq \frac{1}{N}\left[\frac{4(1+|C|^2)}{\beta(1-\beta)}\right], \tag{73}$$

for $N^2 \geq 2/(\beta(1-\beta))$ [24]. Thus, the error in approximating an exact spatially periodic equilibrium solution θ of equation (71) using a finite number of modes approaches zero as the number of modes used becomes large. Furthermore, the smaller β is (for $\beta < 1/2$), the more terms are needed to achieve a given error tolerance, in accord with what one would expect, considering β represents the ratio of the two length scales present in the dynamics.

Restricting the initial conditions for θ and η to be purely real gives the corresponding results for system (1). This is because if we take $\theta_k = \overline{\theta}_{-k}$ and $\eta_k = \overline{\eta}_{-k}$ at $t = 0$, the dynamics (71) maintain this condition for all time. Thus, the conclusion that we obtain for system (1) is that despite the cubic nonlinearity, which results in complicated nonlinear couplings in the modal equations, by considering the complex version of system (1), we are nevertheless able to successfully perform the modal analysis.

5.2. Active Transmission Line

The active transmission line is another system that may be of interest in its own right as well as helping us to better understand system (1). In one spatial dimension, the active transmission line equation takes the form

$$\begin{aligned} \tau_\theta \frac{\partial \theta}{\partial t} &= l^2 \frac{\partial^2 \theta}{\partial x^2} - \theta^3 + \theta - C - L\left(\varepsilon \frac{\partial \eta}{\partial x}\right), \\ \tau_\eta \frac{\partial \eta}{\partial t} &= L^2 \frac{\partial^2 \eta}{\partial x^2} - \eta - L\left(\varepsilon \frac{\partial \theta}{\partial x}\right). \end{aligned} \tag{74}$$

(The control parameter C appears in the θ equation because adding a constant term to the η equation will not influence the θ dynamics.) The reason for calling this system an active transmission line is that when only the coupling terms are retained,

$$\begin{aligned} \tau_\theta \frac{\partial \theta}{\partial t} &= -(\varepsilon L)\frac{\partial \eta}{\partial x}, \\ \tau_\eta \frac{\partial \eta}{\partial t} &= -(\varepsilon L)\frac{\partial \theta}{\partial x}, \end{aligned} \tag{75}$$

the system reduces to the wave equation for a transmission line,

$$\begin{aligned} \frac{\partial^2 \theta}{\partial t^2} &= v^2 \frac{\partial^2 \theta}{\partial x^2}, \\ \frac{\partial^2 \eta}{\partial t^2} &= v^2 \frac{\partial^2 \eta}{\partial x^2}, \end{aligned} \tag{76}$$

where θ represents voltage, η represents current, τ_θ represents capacitance per unit length, τ_η represents inductance per unit length, and $v = \varepsilon L/\sqrt{\tau_\theta \tau_\eta}$ is the speed of traveling solutions. The additional terms in equation (74) add gain and dissipation.

There are two main circuit motivations for using active transmission lines. First, the active elements placed along the length of the transmission line could potentially serve as a simpler and more robust mechanism for overcoming transmission line losses than discrete repeaters. Second, active transmission lines could be used to alleviate fanout problems, because the transmission line only needs to be excited at one end, and then the transmission line itself supplies the power necessary to propagate a pulse along its length [38]. With passive transmission lines, the source needs to be able to drive enough current into each transmission line it is connected to in order to send sufficiently large pulses to the receivers.

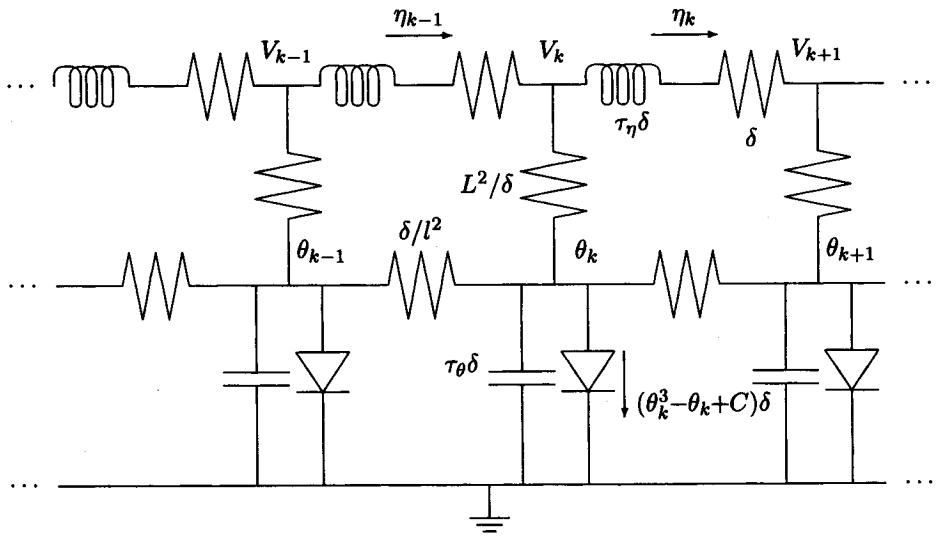

Fig. 10. Active transmission-line circuit with inhibitor diffusion and dissipation. The θ_k are voltages, the η_k are currents, and the diodes represent tunnel diodes (whose biasing circuitry is not shown). The resistors in series with the inductors can be thought of as distributed resistance along the length of the inductors. Parallel resistance associated with the capacitors can be considered to be absorbed into the tunnel diode model. Series resistances (and the capacitances and inductances) scale with δ, and the parallel resistances scale as $1/\delta$.

The active transmission line circuit shown in Figure 10 is a discrete approximation to a lossy transmission line, with additional tunnel diodes. The circuit equations for Figure 10 are

$$\begin{aligned}
\tau_\theta \dot{\theta}_k &= \frac{l^2}{\delta^2}(\theta_{k-1} - 2\theta_k + \theta_{k+1}) - \theta_k^3 + \theta_k - C - \frac{1}{\delta}(\eta_k - \eta_{k-1}), \\
\tau_\theta \dot{\eta}_k &= -\eta_k + \frac{1}{\delta}\left[\theta_k + \frac{L^2}{\delta}(\eta_{k-1} - \eta_k) - \theta_{k+1} - \frac{L^2}{\delta}(\eta_k - \eta_{k+1})\right] \\
&= \frac{L^2}{\delta^2}(\eta_{k-1} - 2\eta_k + \eta_{k+1}) - \eta_k - \frac{1}{\delta}(\theta_{k+1} - \theta_k).
\end{aligned} \tag{77}$$

In the continuum limit (i.e., taking $\delta \to 0$), these equations become system (74) with $\varepsilon L = 1$.

The connection between systems (1) and (74) has to do with the form of the coupling terms. In system (1), the coupling terms are $+\eta$ and $-\theta$, which lead to the indefinite metric associated with the gradient dynamics. In system (74), the coupling terms $-\partial\eta/\partial x$ and $-\partial\theta/\partial x$ also lead to gradient dynamics with an indefinite metric: The term $-\int_\Omega \theta\eta d\mathbf{x}$ in equation (12) is replaced by $\varepsilon L \int_\Omega \theta(\partial\eta/\partial x)dx$. The same approach used in Section 4 can then be applied to system (74), and a Lyapunov functional can be found.

Having a Lyapunov functional for an active transmission line system may seem peculiar, since transmission lines are supposed to have traveling solutions, and Lyapunov functionals indicate that stable states are equilibria. However, the Lyapunov functional

analysis also gives conditions on the parameters, in this case, $\alpha > \varepsilon/2$, to have a valid Lyapunov functional [24]. Thus, for certain parameter values, system (74) acts like a transmission line, and for others, it has a Lyapunov functional.

The implication for system (1) is that we can add coupling terms like those appearing in system (74), and still be able to find a Lyapunov functional. For example, we could take

$$\begin{aligned} \tau_\theta \frac{\partial \theta}{\partial t} &= l^2 \Delta\theta - \theta^3 + \theta + \eta + L(\boldsymbol{\varepsilon} \cdot \nabla\eta), \\ \tau_\eta \frac{\partial \eta}{\partial t} &= L^2 \Delta\eta - \eta - \theta + C + L(\boldsymbol{\varepsilon} \cdot \nabla\theta), \end{aligned} \tag{78}$$

for some constant vector $\boldsymbol{\varepsilon}$, and use the same technique as in Section 4 to find

$$\begin{aligned} V = \int_\Omega \Big[& \frac{l^2}{2}|\nabla\theta|^2 + \frac{1}{4}\theta^4 - \frac{1}{2}\theta^2 + \frac{L^2}{2}|\nabla\eta|^2 + \frac{1}{2}\eta^2 - C\eta + \theta\eta + L\theta(\boldsymbol{\varepsilon} \cdot \nabla\eta) \\ & - (-\theta + L(\boldsymbol{\varepsilon} \cdot \nabla\theta) + C) \\ & \times [(L^2\Delta - 1)^{-1}(-\theta + L(\boldsymbol{\varepsilon} \cdot \nabla\theta) + C)] \Big] d\mathbf{x}. \end{aligned} \tag{79}$$

Further analysis reveals that V is a valid Lyapunov functional as long as $||\boldsymbol{\varepsilon}|| < 1$ and $\alpha > 1$.

Note: In the work of R. S. MacKay, S. Aubry and collaborators (see [39]), the idea of persistence of spatially localized solutions in networks of coupled (linear disordered or nonlinear anharmonic) oscillators is placed on a rigorous mathematical footing. While this is largely a Hamiltonian theory, there are similarities between the limiting cases of active transmission lines and such networks of oscillators that deserve to be further explored.

6. Optical Pattern-Forming System Example

To illustrate how the global nonlinear analysis techniques presented above can be applied to the design of a system containing large microactuator and sensor arrays, we consider an optical pattern-forming system example. Optical pattern-forming systems, and even optical two-component reaction-diffusion equations, have been investigated extensively [7]. Here we ask how the optical pattern-forming system can be designed to ensure global nonlinear stability. If successful, we then have a building block which could potentially be incorporated into a larger control system. The larger control system could be an optical signal processing system, or it could be a feedback system incorporating optical sensing, but performing some other physical task.

An essential feature of the optical implementation we consider is nonlinearity arising from the actuation of optical phase combined with the measurement of optical intensity. There are various microactuator arrays for light which modulate optical phase, for example MEMS piston micromirror arrays [6]. There is also a physical effect in materials, known as the Kerr effect, by which the index of refraction in the material depends locally on the incident optical intensity. For a thin slice of such material (called a Kerr slice),

the phase shift distribution imposed on a light beam by the Kerr slice is related to the intensity distribution of the beam at the Kerr slice. Although the Kerr effect is too weak in practical materials to be of much use, a liquid-crystal light valve (LCLV) can implement the functionality of a Kerr slice in a practical system [7]. LCLV devices for this purpose consist of a photoconductive layer, glass layers which hold the liquid crystals in place, and transparent bias electrodes. The optical intensity distribution incident on the photoconductive layer modulates the conductivity, which in turn changes the bias across the liquid crystal layer, causing the liquid crystal molecules to reorient. The orientation of the liquid crystal molecules determines how much phase shift is imposed on the light (linearly polarized, with appropriate axis of polarization) passing through the device. For approximating a Kerr slice, LCLV devices currently offer higher resolution than MEMS devices. (Rather than deal with the details of LCLV devices, we will take the common approach of analyzing systems with Kerr slices.)

Although actuation of optical phase is straightforward, optical phase cannot be sensed directly. An interferometer creates an intensity distribution related to a beam's phase distribution by coherent superposition with a reference beam. However, the intensity distribution which results is actually a sinusoidal function of the original phase distribution. There are also phase-contrast approaches, which yield intensity distributions that are nonlinear functionals of phase, that do not require a reference beam as the interferometer does. One of these phase-contrast techniques, the differential Zernike filter, provides a phase-to-intensity mapping that is particularly well-suited to the problem of design for global nonlinear stability [27], [28]. To keep the analysis as simple as possible, here we will consider an interferometer for phase measurement.

6.1. Rescaled Dynamics

One feature of equation (1) which plays an intrinsic role in the stability analysis is the linearity of the cross-coupling terms between the activator equation and inhibitor equation. For our optical pattern-forming system, it is important to understand how the global nonlinear analysis might be able to accomodate nonlinearity in this cross-coupling. Remarkably, it can, but we first need to rescale the dynamics.

A slightly modified version of system (1) is

$$\begin{aligned} \tau_\theta \frac{\partial \theta}{\partial t} &= l^2 \Delta\theta - \theta^3 + \theta + \eta + C, \\ \tau_\eta \frac{\partial \eta}{\partial t} &= L^2 \Delta\eta - \eta - \theta - \delta C, \end{aligned} \tag{80}$$

where δ is a positive constant. All of the qualitative properties and mathematical results for system (1) also hold for system (80). System (80) can be rescaled into the form

$$\begin{aligned} \tau_{\theta o} \frac{\partial \theta_o}{\partial t} &= l_o^2 \Delta\theta_o - \theta_o^3 - \frac{\gamma}{1+\gamma}\theta_o + \gamma\theta_o + \gamma\eta_o + \gamma C_o, \\ \tau_{\eta o} \frac{\partial \eta_o}{\partial t} &= L_o^2 \Delta\eta_o - \eta_o - \gamma\theta_o - \gamma\eta_o - \gamma C_o, \end{aligned} \tag{81}$$

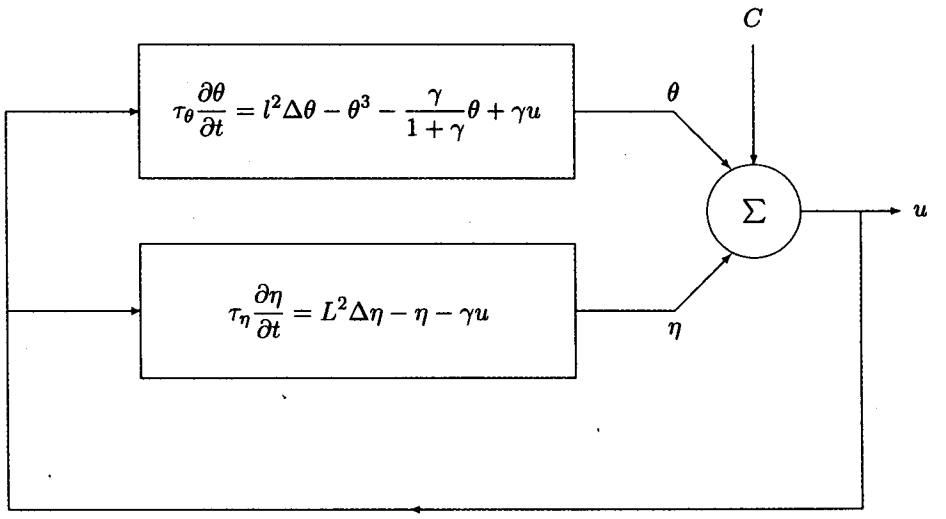

Fig. 11. Block diagram of the rescaled activator-inhibitor system with a common feedback signal driving both the activator and inhibitor equations.

using

$$\begin{aligned}
\tau_\theta &= \frac{1+\gamma}{\gamma^2}\tau_{\theta o}, \qquad \tau_\eta = \frac{1}{1+\gamma}\tau_{\eta o}, \qquad l = \frac{\sqrt{1+\gamma}}{\gamma} l_o, \qquad L = \frac{1}{\sqrt{1+\gamma}} L_o, \\
\theta &= \frac{\sqrt{1+\gamma}}{\gamma}\theta_o, \qquad \eta = \frac{(\sqrt{1+\gamma})^3}{\gamma^2}\eta_o, \qquad C = \frac{(\sqrt{1+\gamma})^3}{\gamma^2} C_o, \\
\delta &= \frac{\gamma}{1+\gamma}.
\end{aligned} \tag{82}$$

System (81) can be expressed as a feedback system with a single feedback signal driving both the activator and inhibitor equations:

$$\begin{aligned}
\tau_{\theta o}\frac{\partial \theta_o}{\partial t} &= l_o^2 \Delta\theta_o - \theta_o^3 - \frac{\gamma}{1+\gamma}\theta_o + \gamma u, \\
\tau_{\eta o}\frac{\partial \eta_o}{\partial t} &= L_o^2 \Delta\eta_o - \eta_o - \gamma u, \\
u &= \theta_o + \eta_o + C_o,
\end{aligned} \tag{83}$$

where we are thinking of C_o as an exogenous input signal. Figure 11 shows a block diagram of system (83), where we have dropped the "o" subscripts.

For the implementation shown in Figure 11, there is a single spatially varying feedback signal u, which also incorporates the exogenous input, and this single feedback signal drives both the state equation for θ and the state equation for η. We can think of u as being the signal we have access to (for purposes of controlling a microactuator array, for example), while θ and η need not be directly available.

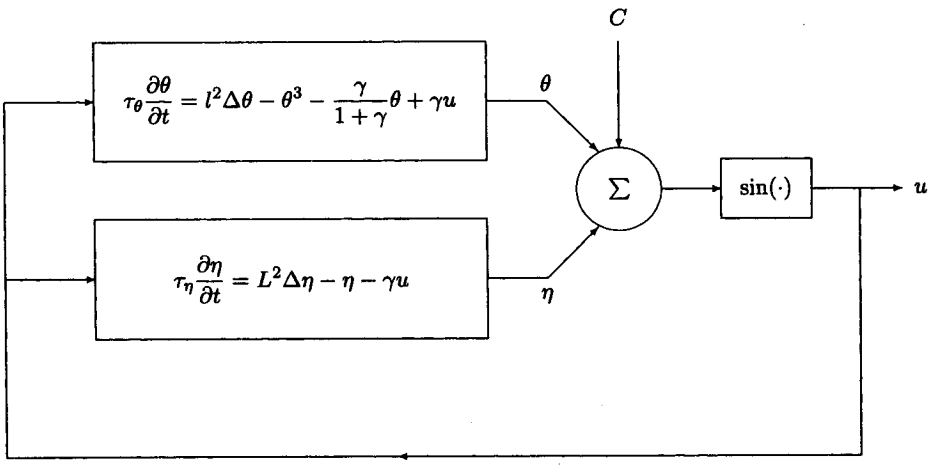

Fig. 12. Block diagram of the (rescaled) activator-inhibitor system with a sinusoidal nonlinearity in the feedback path.

In Figure 11, the inhibitor equation represents a typical linear model for a Kerr slice, with optical phase shift represented by η and controlling intensity represented by u [7]. Similarly, except for the θ^3 term, the activator equation also represents a linear Kerr slice, the difference being that the dependence of steady-state phase shift on controlling intensity has the opposite sign of that for the inhibitor Kerr slice. In optics terminology, the activator Kerr slice consists of "focusing" media, and the inhibitor Kerr slice consists of "defocusing" media. Because of the θ^3 term in the activator equation, we are assuming a particular nonlinear Kerr response for the activator Kerr slice.

6.2. Feedback Path Nonlinearity

We now introduce the nonlinearity in the feedback path due to the interferometric measurement of phase. We will assume that the interferometer has been adjusted so that the intensity can be represented as a purely sinusoidal function of phase (we drop the spatially uniform additive component of the interferometer intensity distribution, since it plays no essential role). Figure 12 corresponds to the following dynamics:

$$\begin{aligned} \tau_\theta \frac{\partial \theta}{\partial t} &= l^2 \Delta \theta - \theta^3 - \frac{\gamma}{1+\gamma}\theta + \gamma \sin(\theta + \eta + C), \\ \tau_\eta \frac{\partial \eta}{\partial t} &= L^2 \Delta \eta - \eta - \gamma \sin(\theta + \eta + C), \end{aligned} \tag{84}$$

where $0 < \gamma < 1/2$. The relationship between system (84) and system (80) is as follows: If we assume θ, η, and C in system (84) are small enough, we can approximate $\sin(\theta + \eta + C)$ by simply $(\theta + \eta + C)$, and we obtain system (81), which differs from system (80) only by a rescaling. (We have introduced the exogenous input C before instead of after the nonlinearity, but this choice was arbitrary.)

We can use the same technique as in Section 4 to find

$$V = \int_\Omega \left[\frac{l^2}{2}|\nabla\theta|^2 + \frac{1}{4}\theta^4 + \frac{1}{2}\left(\frac{\gamma}{1+\gamma}\right)\theta^2 + \gamma\cos(\theta+\eta+C) + \frac{L^2}{2}|\nabla\eta|^2 + \frac{1}{2}\eta^2 \right.$$
$$+ 2\gamma\eta\sin(\theta+\eta+C) - \gamma\sin(\theta+\eta+C)$$
$$\left. \times\ [(L^2\Delta - 1)^{-1}(\gamma\sin(\theta+\eta+C))] \right] d\mathbf{x}, \tag{85}$$

which is a valid Lyapunov functional for system (84) provided $\gamma < 1/2$, and $\alpha = \tau_\theta/\tau_\eta > \gamma^2/(1-2\gamma)$.

6.3. Dynamics with Advection

Once we have excited stable localized equilibrium structures in our activator-inhibitor system, we would like to be able to translate them (for example, to manipulate objects atop an actuator array). For purposes of illustration, let us temporarily take $\alpha = 1$ so that we can rescale t to set $\tau_\theta = \tau_\eta = 1$. The simplest modification to system (80) to achieve translation of the stable localized equilibrium structures is the addition of advective terms to both the activator and inhibitor dynamics:

$$\frac{\partial\theta}{\partial t} = l^2\Delta\theta - \theta^3 + \theta + \eta + C + L(\boldsymbol{\varepsilon}\cdot\nabla\theta),$$
$$\frac{\partial\eta}{\partial t} = L^2\Delta\eta - \eta - \theta - \delta C + L(\boldsymbol{\varepsilon}\cdot\nabla\eta), \tag{86}$$

where $\boldsymbol{\varepsilon}$ is a constant control vector determining the speed and direction of translation. Then changing to the translating frame of reference

$$\psi(\mathbf{x},t) = \theta(\mathbf{x} - \boldsymbol{\varepsilon}Lt, t),$$
$$\zeta(\mathbf{x},t) = \eta(\mathbf{x} - \boldsymbol{\varepsilon}Lt, t), \tag{87}$$

we obtain

$$\frac{\partial\psi}{\partial t} = -L(\boldsymbol{\varepsilon}\cdot\nabla\theta) + \frac{\partial\theta}{\partial t},$$
$$\frac{\partial\zeta}{\partial t} = -L(\boldsymbol{\varepsilon}\cdot\nabla\eta) + \frac{\partial\eta}{\partial t}, \tag{88}$$

and hence

$$\frac{\partial\psi}{\partial t} = l^2\Delta\psi - \psi^3 + \psi + \zeta + C,$$
$$\frac{\partial\zeta}{\partial t} = L^2\Delta\zeta - \zeta - \psi - \delta C, \tag{89}$$

which is identical to system (80).

A slightly more complicated system with advection is

$$\frac{\partial\theta}{\partial t} = l^2\Delta\theta - \theta^3 + C + (\theta + \eta + L(\boldsymbol{\varepsilon}\cdot\nabla\theta) + L(\boldsymbol{\varepsilon}\cdot\nabla\eta)),$$
$$\frac{\partial\eta}{\partial t} = L^2\Delta\eta - \delta C + (-\theta - \eta + L(\boldsymbol{\varepsilon}\cdot\nabla\theta) + L(\boldsymbol{\varepsilon}\cdot\nabla\eta)), \tag{90}$$

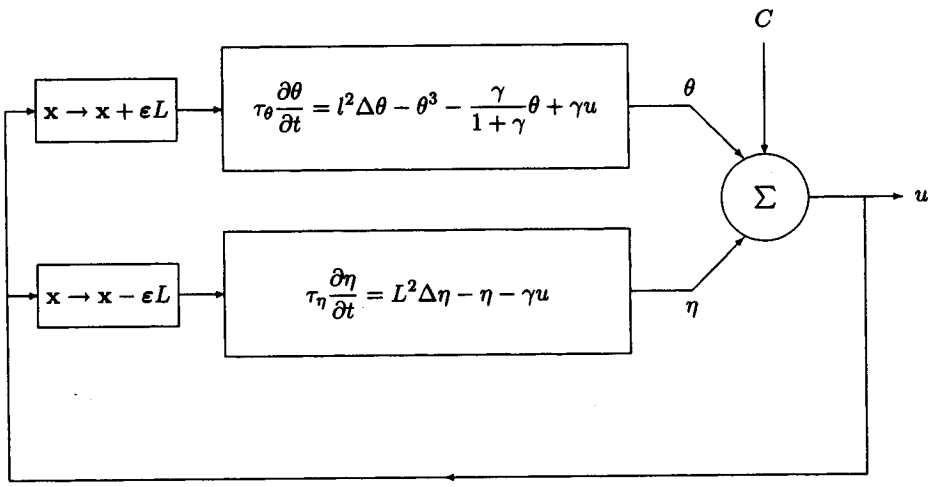

Fig. 13. Block diagram of the (rescaled) activator-inhibitor system with spatially shifted feedback.

where we have grouped together the terms associated with cross-coupling between the two equations. If we again change to the translating frame of reference given by equation (87), we obtain

$$\begin{aligned} \frac{\partial \psi}{\partial t} &= l^2 \Delta \psi - \psi^3 + \psi + \zeta + C + L(\varepsilon \cdot \nabla \zeta), \\ \frac{\partial \zeta}{\partial t} &= L^2 \Delta \zeta - \zeta - \psi - \delta C + L(\varepsilon \cdot \nabla \psi), \end{aligned} \tag{91}$$

and this system is identical to system (78), except for the control parameter entering in a slightly different way. Therefore, system (91) has the same basic behavior as system (80) for $||\varepsilon||$ sufficiently small (i.e., a Lyapunov functional exists).

System (90) arises by spatially translating the feedback terms and then using a Taylor-series approximation. The system with translated feedback is

$$\begin{aligned} \frac{\partial \theta}{\partial t}(\mathbf{x}, t) &= l^2 \Delta \theta(\mathbf{x}, t) - (\theta(\mathbf{x}, t))^3 + C + \theta(\mathbf{x} + \varepsilon L, t) + \eta(\mathbf{x} + \varepsilon L, t), \\ \frac{\partial \eta}{\partial t}(\mathbf{x}, t) &= L^2 \Delta \eta(\mathbf{x}, t) - \delta C - \theta(\mathbf{x} - \varepsilon L, t) - \eta(\mathbf{x} - \varepsilon L, t), \end{aligned} \tag{92}$$

which for small $||\varepsilon||$ is approximately system (90). Physically, system (92) corresponds to spatially shifting the feedback signal slightly in one direction for the θ dynamics, and the same amount in the opposite direction for the η dynamics. Figure 13 illustrates the spatially shifted feedback, and corresponds to the system

$$\begin{aligned} \tau_\theta \frac{\partial \theta}{\partial t} &= l^2 \Delta \theta - \theta^3 - \frac{\gamma}{1+\gamma} \theta + \gamma \theta + \gamma \eta + \gamma C + \gamma L(\varepsilon \cdot \nabla \theta) + \gamma L(\varepsilon \cdot \nabla \eta), \\ \tau_\eta \frac{\partial \eta}{\partial t} &= L^2 \Delta \eta - \eta - \gamma \theta - \gamma \eta - \gamma C + \gamma L(\varepsilon \cdot \nabla \theta) + \gamma L(\varepsilon \cdot \nabla \eta), \end{aligned} \tag{93}$$

where we have assumed that C is constant. System (93) can be rescaled into the form

$$\tau_\theta \frac{\partial \theta}{\partial t} = l^2 \Delta\theta - \theta^3 + \theta + \eta + \frac{1+\gamma}{\gamma} L(\varepsilon \cdot \nabla\theta) + L(\varepsilon \cdot \nabla\eta) + C,$$
$$\tau_\eta \frac{\partial \eta}{\partial t} = L^2 \Delta\eta - \eta - \theta + L(\varepsilon \cdot \nabla\theta) + \frac{\gamma}{1+\gamma} L(\varepsilon \cdot \nabla\eta) - \delta C. \tag{94}$$

We can change to the translating frame of reference and obtain a system corresponding to (91), provided

$$\alpha = \frac{\tau_\theta}{\tau_\eta} = \frac{(1+\gamma)/\gamma}{\gamma/(1+\gamma)} = \left(\frac{1+\gamma}{\gamma}\right)^2. \tag{95}$$

7. Summary and Conclusions

We have examined an activator-inhibitor equation with a cubic nonlinearity as a model pattern-forming system for control of large actuator arrays. We have described in broad terms how pattern-forming systems could be used to control large actuator arrays through interconnection templates and a control parameter which stresses the interconnections (leading to the crossing of stability thresholds). We have shown that there are some interesting mathematical results that can be derived for the activator-inhibitor system, and that the results generalize to two other systems, the complex activator-inhibitor equation and the active transmission line. We have also described a general approach for optical implemention of the activator-inhibitor equations, and have shown that in spite of the intrinsic nonlinearities that arise in optics, the global nonlinear convergence behavior can still hold.

In addition to the generalizations of the cubic nonlinearity activator-inhibitor equation we have presented, it should be noted that the results can also be extended to higher-order nonlinearities in the activator equation. The higher-order Lyapunov functional is straightforward to write down; however, the modal equations presented in Section 5.1 will become much more complicated. Spatially varying coefficients (subject to appropriate bounds) in equation (1) can also be accommodated by the Lyapunov functional analysis, which is important for analog implementations subject to component nonuniformities.

It is only now becoming technologically feasible to construct arrays of sensors and actuators which are so large that centralized processing is infeasible. Pattern-forming systems are a natural approach for easing the demands on a centralized processor. While there has been extensive theoretical and experimental work on pattern-forming systems that arise in physics, chemistry, and biology, such systems have not yet been exploited in control of engineering systems.

This work illustrates that even though pattern-forming systems are coupled systems of nonlinear PDEs, in some cases it is still possible to obtain the types of mathematical results that can ensure global convergence. Furthermore, these systems are still rich enough to provide an interesting family of stable (or metastable) states, including spikes, walls, symmetric patterns, and disordered patterns. As actuator array technology improves and array sizes increase, control issues will need to be considered as an integral part of the

actuator array design. The convergence results presented here should be thought of as a possible starting point for this design process.

Appendix: Proof of Theorem 3

The proof of Theorem 3 is essentially the same as the proof of a similar theorem given in [34], [35]. We include the proof because it does not appear to be widely known within the controls community. For example, although the result is mentioned as a footnote in [40], no reference to a proof is given.

Proof. Let L^+ denote the positive limit set of $\nu(t)$. Since $\nu(t) \in \Sigma$, a compact set, $\forall t \geq 0$, we have that L^+ is a nonempty, compact, invariant set [33]. Therefore, $\exists \nu^* \in L^+$, and a sequence $\{t_n\}$, such that $\lim_{t\to\infty} \nu(t_n) = \nu^*$. Furthermore, since J is positive definite, $\dot{V} = 0$ if and only if $f(\nu) = 0$, so from Theorem 1 it follows that $V(\nu(t)) \geq V(\nu^*)$, $\forall t \geq 0$. Now we apply the Lojasiewicz lemma: at ν^*, $\exists U \subset \Sigma$ and $\mu \in (0, 1)$ such that

$$(V(\nu) - V(\nu^*))^\mu \leq |\nabla V(\nu)|, \qquad \forall \nu \in U. \tag{96}$$

Choose r such that $B_{3r}(\nu^*) \subset U$ (where $B_{3r}(\nu^*)$ denotes the ball of radius $3r$ centered at ν^*). Since $\nu^* \in L^+$ and V is continuous, $\exists t_1 > 0$ such that $\nu(t_1) \in B_r(\nu^*)$, and

$$(V(\nu(t_1)) - V(\nu^*))^{1-\mu} < (1-\mu)r. \tag{97}$$

For $\nu \in B_{3r}(\nu^*) \subset U$,

$$\begin{aligned} |\dot{\nu}| &= |J^{-1}\nabla V| \leq |J^{-1}| \frac{|\nabla V|^2}{|\nabla V|} \leq \frac{|J^{-1}|}{\min \lambda(J^{-1})_{sym}} \left(\frac{-\dot{V}}{|\nabla V|}\right) \\ &\leq \frac{|J^{-1}|}{\min \lambda(J^{-1})_{sym}} \left(\frac{-\dot{V}}{(V(\nu) - V(\nu^*))^\mu}\right) \\ &= \frac{|J^{-1}|}{\min \lambda(J^{-1})_{sym}} \left(\frac{-1}{1-\mu}\right) \frac{d}{dt}(V(\nu) - V(\nu^*))^{1-\mu}, \end{aligned} \tag{98}$$

where $\min \lambda(J^{-1})_{sym}$ denotes the smallest eigenvalue of the symmetric part of J^{-1} (which is positive, because J is positive definite). Now suppose $\nu(t)$ does not stay in $B_{3r}(\nu^*)$, $\forall t > t_1$. Then $\exists t_2$ such that

$$3r \leq |\nu(t_2) - \nu^*| \leq |\nu(t_2) - \nu(t_1)| + |\nu(t_1) - \nu^*| \leq |\nu(t_2) - \nu(t_1)| + r, \tag{99}$$

and so

$$\begin{aligned} 2r &\leq |\nu(t_2) - \nu(t_1)| = \left| \int_{t_1}^{t_2} \frac{d\nu}{d\tau} d\tau \right| \leq \int_{t_1}^{t_2} \left| \frac{d\nu}{d\tau} \right| d\tau \\ &\leq \left(\frac{-1}{1-\mu}\right) \int_{t_1}^{t_2} \frac{d}{d\tau} \left(V(\nu) - V(\nu^*)\right)^{1-\mu} d\tau \end{aligned}$$

$$= \frac{1}{1-\mu}\left[(V(\nu(t_1)) - V(\nu^*))^{1-\mu} - (V(\nu(t_2)) - V(\nu^*))^{1-\mu}\right]$$

$$\leq \frac{1}{1-\mu}(V(\nu(t_1)) - V(\nu^*))^{1-\mu}. \tag{100}$$

However, equation (100) contradicts equation (97), and therefore $\nu(t) \in B_{3r}(\nu^*)$, $\forall t > t_1$. Finally, from equation (100) we see that

$$\int_{t_1}^{\infty} \left|\frac{d\nu}{d\tau}\right| d\tau \leq \frac{1}{1-\mu}(V(\nu(t_1)) - V(\nu^*))^{1-\mu} < \infty, \tag{101}$$

so the trajectory $\nu(t)$ has finite Euclidean length. Therefore, $\lim_{t\to\infty} \nu(t) = \nu^*$ [34], [35], [36]. □

Acknowledgments

This research was supported in part by a grant from the Army Research Office under the ODDR&E MURI97 Program Grant No. DAAG55-97-1-0114 to the Center for Dynamics and Control of Smart Structures (through Harvard University). The authors would also like to thank Mikhail Vorontsov for valuable discussions.

References

[1] K. F. Bohringer and B. R. Donald, "Algorithmic MEMS," *Robotics, the Algorithmic Perspective; The Third Workshop on the Algorithmic Foundations of Robotics*, P. K. Agarwal, L. E. Kavraki, and M. T. Mason, eds., pp. 1–20, A. K. Peters Publ., Natick, MA, 1998.

[2] E. W. Justh and P. S. Krishnaprasad, "Analysis of a complex activator-inhibitor equation," *Proceedings of the American Control Conference*, pp. 1613–1617, 1999 (also ISR TR 99-13).

[3] K. P. Selverov and H. A. Stone, "Peristaltically Driven Flows for Micro-Mixers," *Proceedings of the MEMS '98*, L. Lin, F. K. Foster, N. R. Aluru, and X. Zhang, eds., DSC-Vol. 66, ASME, New York, 1998.

[4] K. P. Selverov and H. A. Stone, "Peristaltically driven flows with applications towards micromixing," *Physics of Fluids*, Vol. 13, No. 7, pp. 1837–1859, 2001.

[5] J. Lumley and P. Blossey, "Control of Turbulence," *Annual Review of Fluid Mechanics*, Vol. 30, pp. 311–327, 1998.

[6] T. G. Bifano, J. Perreault, R. K. Mali, and M. N. Horenstein, "Microelectromechanical Deformable Mirrors," *IEEE Journal of Selected Topics in Quantum Electronics*, Vol. 5, No. 1, pp. 83–89, 1999.

[7] M. A. Vorontsov and W. B. Miller. *Self-organization in Optical Systems and Applications in Information Technology*, 2nd ed., Springer-Verlag, New York, 1998.

[8] M. C. Cross and P. C. Hohenberg, "Pattern formation outside of equilibrium," *Reviews of Modern Physics*, Vol. 65, No. 3, pp. 851–1112, 1993.

[9] G. B. Ermentrout and J. D. Cowan, "A mathematical theory of visual hallucination patterns," *Biological Cybernetics*, Vol. 34, No. 3, pp. 137–150, 1979.

[10] J. D. Murray, *Mathematical Biology*, 2nd ed., Springer-Verlag, New York, 1993.

[11] A. T. Winfree, *The Geometry of Biological Time*, 2nd ed., Springer-Verlag, New York, 2000.

[12] G. Li, Q. Ouyang, V. Petrov, and H. L. Swinney, "Transition from Simple Rotating Chemical Spirals to Meandering and Traveling Spirals," *Physical Review Letters*, Vol. 77, No. 10, pp. 2105–2108, 1996.

[13] M. Sheintuch and S. Shvartsman, "Spatiotemporal patterns in Catalytic Reactor: Journal Review," *American Institute of Chemical Engineers Journal*, Vol. 42, No. 4, pp. 1041–1068, 1996.
[14] M. Bar, I. G. Kevrekidis, H. H. Rotermund, and G. Ertl, "Pattern formation in composite excitable media," *Physical Review E*, Vol. 52, No. 6, pp. R5739–R5742, 1995.
[15] P. B. Umbanhowar, F. Melo, and H. L. Swinney, "Localized excitations in a vertically vibrated granular layer," *Nature*, Vol. 382, pp. 793–796, 1996.
[16] M. Bode and H.-G. Purwins, "Pattern formation in reaction-diffusion systems: Dissipative solitons in physical systems," *Physica D*, Vol. 86, pp. 53–63, 1995.
[17] B. S. Kerner and V. V. Osipov, "Autosolitons," *Soviet Physics Uspekhi*, Vol. 32, No. 2, pp. 101–138, 1989.
[18] B. S. Kerner and V. V. Osipov, *Autosolitons*, Kluwer Academic Publishers, Boston, 1994.
[19] M. Barahona, E. Trias, T. P. Orlando, A. E. Duwel, H. S. J. van der Zant, S. Watanabe, and S. H. Strogatz, "Resonances of dynamical checkerboard states in Josephson arrays with self-inductance," *Physical Review B*, Vol. 55, No. 18, pp. 11,989–11,992, 1997.
[20] K. Y. Tsang, R. E. Mirollo, S. H. Strogatz, and K. Wiesenfeld, "Dynamics of a Globally Coupled Oscillator Array," *Physica D*, Vol. 48, pp. 102–112, 1991.
[21] C. P. Schenk, P. Schutz, M. Bode, and H.-G. Purwins, "Interaction of self-organized quasiparticles in a two-dimensional reaction-diffusion system: The formation of molecules," *Physical Review E*, Vol. 57, No. 6, pp. 6480–6486, 1998.
[22] H.-G. Purwins and Ch. Radehaus, "Pattern Formation on Analogue Parallel Networks," *Neural and Synergetic Computers*, Hermann Haken, ed., pp. 137–154, Springer-Verlag, Berlin, 1988.
[23] S. C. Zhu and D. Mumford, "Prior Learning and Gibbs Reaction-Diffusion," *IEEE Transactions on Pattern Analysis and Machine Intelligence*, Vol. 19, No. 11, pp. 1236–1250, 1997.
[24] E. W. Justh, *Control of Large Actuator Arrays Using Pattern-Forming Systems*, Ph.D. dissertation, University of Maryland, ISR Ph.D. Thesis Report 98-6, 1998 (see http://www.isr.umd.edu/TechReports/ISR/1998).
[25] E. W. Justh and P. S. Krishnaprasad, "A Lyapunov functional for the cubic nonlinearity activator-inhibitor model equation," *Proceedings of the IEEE Conference on Decision and Control*, pp. 1404–1409, IEEE, New York, 1998 (also ISR TR 98-36).
[26] J. L. Lions, "On the controllability of distributed systems," *Proceedings of the National Academy of Sciences, USA*, Vol. 94, pp. 4828–4835, 1997.
[27] E. W. Justh, P. S. Krishnaprasad, and M. A. Vorontsov, "Nonlinear Analysis of a High-Resolution Optical Wavefront Control System," *Proceedings of the 39th IEEE Conference on Decision and Control*, pp. 3301–3306, IEEE, New York, 2000.
[28] E. W. Justh, M. A. Vorontsov, G. W. Carhart, L. A. Beresnev, and P. S. Krishnaprasad, "Adaptive Optics with Advanced Phase-Contrast Techniques: Part II. High-Resolution Wavefront Control," *Journal of the Optical Society of America A*, Vol. 18, No. 6, pp. 1300–1311, 2001.
[29] L. C. Evans. *Partial Differential Equations*. American Mathematical Society, Providence, RI, 1998.
[30] R. Temam. *Infinite-Dimensional Dynamical Systems in Mechanics and Physics*, 2nd ed. Springer-Verlag, New York, 1997.
[31] R. K. Brayton and J. K. Moser, "A Theory of Nonlinear Networks—I," *Quarterly of Applied Mathematics*, Vol. XXII, No. 1, pp. 1–33, 1964.
[32] P. B. Gilkey. *The Index Theorem and the Heat Equation*. Mathematics Lecture Series 4, Publish or Perish, Inc., Boston, 1974.
[33] H. Khalil. *Nonlinear Systems*. Macmillan Publishing Co., New York, 1992.
[34] R. Mahony, "Convergence of Gradient Flows and Gradient Descent Algorithms for Analytic Cost Functions," *Proceedings of the International Symposium MTNS-98*, 1998.
[35] R. E. Mahony and B. Andrews, "Convergence of the Iterates of Descent Methods for Analytic Cost Function," Preprint, 1999.
[36] S. P. Bhat and D. S. Bernstein, "Lyapunov Analysis of Semistability," *Proceedings of the American Control Conference*, pp. 1608–1612, 1999.

[37] S. Lojasiewicz, "Ensembles semi-analytiques," Technical Report, Institut des Hautes Etudes Scientifiques, Bures-sur-Yvette (Sein-et-Oise), France, 1965.
[38] L. Cauler and A. Penz, "Neurointeractivism: Emergence by Real-Time Environmental Dynamics," Neuromorphic VLSI PI Meeting, Naval Research Laboratory, Washington, DC, June 23–24, 1998.
[39] J. F. R. Archilla, R. S. MacKay, and J. L. Marin, "Discrete breathers and Anderson modes: Two faces of the same phenomenon?" *Physica D*, Vol. 134, pp. 406–418, 1999.
[40] M. W. Hirsch, "Convergent Activation Dynamics in Continuous Time Networks," *Neural Networks*, Vol. 2, pp. 331–349, 1989.